Analyzing Selected Mapping for Peak-to-Average Power Reduction in OFDM

A Thesis
Presented to
The Academic Faculty

by

Robert J. Baxley

In Partial Fulfillment
of the Requirements for the Degree
Master of Science in Electrical Engineering

School of Electrical and Computer Engineering
Georgia Institute of Technology
May 2005

Analyzing Selected Mapping for Peak-to-Average Power Reduction in OFDM

Approved by:

Professor G. Tong Zhou, Advisor
School of Electrical and Computer Engineering
Georgia Institute of Technology

Professor J. Stevenson Kenney
School of Electrical and Computer Engineering
Georgia Institute of Technology

Professor Ye (Geoffrey) Li
School of Electrical and Computer Engineering
Georgia Institute of Technology

Date Approved: April 14, 2005

To my mom and dad.

ACKNOWLEDGEMENTS

I would like to express my gratitude toward those who have supported me through the thesis process. First, I would like give my sincerest thanks to my advisor, Dr. G. Tong Zhou, for her unreserved guidance, support and encouragement. She has looked out for me at every turn and has given me every opportunity to succeed; for that, I am truly grateful. I consider myself lucky to be one of her students. I want to thank my thesis committee, Dr. Kenney and Dr. Li, for taking the time to review and critique my work. Additionally, I would like to thank my fellow research group members for their friendship and insightful comments along the way. Finally, I want to thank my family, who have supported me through ever step of my life.

TABLE OF CONTENTS

LIST OF TABLES

LIST OF FIGURES

LIST OF SYMBOLS OR ABBREVIATIONS

Symbols

$((\cdot))_N$	modulo N of argument
$(*)_N$	circular convolution of length N
$\circ$	element-wise vector multiplication
$cum[\cdot]$	cumulant
D	number of mapping in SLM
$DFT\{\cdot\}$	DFT (output is indexed on k)
$E[\cdot]$	expected value
f_c	carrier frequency
γ_o	clipping level
$h[n]$	channel impulse response
$IDFT_L\{\cdot\}$	L times oversampled IDFT (output is indexed on n)
L	oversampling factor
N	number of OFDM subcarriers
x	generalization of time domain OFDM symbol
$X[k]$	frequency-domain constellation points
$\boldsymbol{X}$	vector of N frequency-domain constellation points
$x[n/L]$	discrete-time samples of an OFDM symbol
$\boldsymbol{x}_L$	vector of the NL discrete-time samples from an ODFM symbol
$x^{(d)}$	d^{th} mapping of signal x
$x_{n/L}$	discrete-time samples of an OFDM symbol
X_k	frequency-domain constellation points

Abbreviations

ACE	active constellation extension
AWGN	additive white Gaussian noise
BER	bit error rate
BSLM	blind selected mapping
BSPTM	blind selected pilot tone modulation
CCDF	complementary cumulative distribution function
CDF	cumulative distribution function
CF	crest factor
CFR	crest factor reduction
CP	cyclic prefix
CSI	channel state information
DAB	digital audio broadcasting
DAC	digital-to-analog converter
DER	detection error rate
DFT	digital fourier transform
DSL	digital subscriber line
DSLM	dynamic selected mapping
DSP	digital signal processing
EIRP	effective eradiated power
FCC	Federal Communications Commission
FFT	fast fourier transform
HDSL	high-bit-rate digital subscriber lines
HVHDSL	very high speed digital subscriber lines
i.i.d.	independent identically distributed
ICI	inter-carrier interference
IDFT	inverse digital fourier transform
IEEE	Institute of Electrical and Electronics Engineers

IFFT	inverse fast fourier transform
ISI	inter-symbol interference
LDPC	low-density parity check code
MAP	maximum a posteriori
ML	maximum likelihood
MMDS	multicarrier multipoint distribution service
OFDM	orthogonal frequency division multiplexing
OVSF	orthogonal variable spreading factor
PA	power amplifier
PAPR	peak-to-average power ratio
PAR	peak-to-average ratio
PICR	peak interference-to-carrier ratio
PMEPR	peak to mean envelope power ratio
POCS	projection onto convex sets
PSK	phase shift keying
PSNR	peak signal-to-noise ratio
PTAM	pilot tone assisted modulation
PTS	partial transmit sequence
QAM	quadrature amplitude modulation
SER	symbol error rate
SLM	selected mapping
SNDR	signal to noise plus distortion ratio
SNR	signal-to-noise ratio

SUMMARY

Orthogonal frequency division multiplexing (OFDM) has become a popular modulation method in high-speed wireless communications. By partitioning a wideband fading channel into flat narrowband channels, OFDM is able to mitigate the detrimental effects of multipath fading using a simple one-tap equalizer. However, in the time domain OFDM signals suffer from large envelope variations, which are often characterized by the peak-to-average ratio (PAR). High PAR signals, like OFDM, require that transmission amplifiers operate at very low power efficiencies to avoid clipping.

In this thesis we review the most popular OFDM PAR-reduction techniques and demonstrate that selected mapping (SLM) is a particularly promising reduction technique. In a SLM system, an OFDM symbol is mapped to a set of quasi-independent equivalent symbols and then the lowest-PAR symbol is selected for transmission. The tradeoff for PAR reduction in SLM is computational complexity as each mapping requires an additional inverse fast fourier transform (IFFT) operation in the transmitter.

In additional to an overview of current SLM work, we present a thorough analysis of SLM as well as several novel SLM proposals. First, we derive the closed-form expression for the expected PAR in an SLM system. The expected PAR can be thought of as a metric of PAR reduction capability. Second, we provide a power analysis of SLM to determine if the computational power costs outweigh the power saved through PAR reduction. Through this analysis, we show that SLM is capable of several Watts of net power savings when used in a wireless transmission system. Third, we propose that a PAR threshold should be set in SLM. Such thresholding leads to significant complexity decreases. Fourth, we derive the maximum likelihood (ML) and maximum *a posteriori* (MAP) detection metrics for blind SLM (BSLM) and threshold BSLM respectively. Lastly, we demonstrate that by using monomial phase sequences in SLM blind phase sequence detection is possible with a single FFT operation in the receiver.

CHAPTER I

PEAK-TO-AVERAGE RATIO IN ORTHOGONAL FREQUENCY DIVISION MULTIPLEXING

OFDM, first discussed in the mid-1960s [17] and later patented in 1970 [18], is a popular method of high-speed data transmission. Early on, OFDM's main appeal was that high-speed equalization was not necessary because data was sent in parallel on different subcarriers. OFDM was also touted for its ability to fully use the available bandwidth, combat impulsive noise and mitigate the effects of multipath fading.

In 1971 Weinstein and Ebert introduced the idea of using the discrete Fourier transform in the modulation/demodulation process [66]. Prior to this breakthrough, OFDM systems were prohibitively complex because arrays of sinusoidal generators and coherent demodulators were necessary in the implementation. With special-purpose fast Fourier transform (FFT) chips, the entire OFDM system could be implemented digitally.

More recently, OFDM has been implemented in mobile wideband data transmission (IEEE 802.11a, Hiperlan II), high-bit-rate digital subscriber lines (HDSL), asymmetric digital subscriber lines (ADSL), very high-speed digital subscriber lines (VHDSL), digital audio broadcasting (DAB), digital television and high-definition television (HDTV) [73]. It is also the implemented for the IEEE 802.16 WiMAX [2] standard and its predecessor multicarrier multipoint distribution service (MMDS).

Despite the widespread acceptance of OFDM, it has its drawbacks. One drawback is that OFDM systems are not robust again carrier frequency estimation errors. Even small carrier offsets destroy the orthogonality between the subcarriers causing drastic error rate increases [49][55][6][41]. The second drawback is that OFDM signals suffer from large envelope variations. Such variations are problematic because practical communication systems are peak power limited. Thus, envelope peaks require a system to accommodate an instantaneous signal power that is larger than the signal average power, necessitating either low

operating power efficiencies or power amplifier (PA) saturation.

In this chapter, first we will provide an introduction to the details of OFDM. Next, we will define the peak-to-average ratio (PAR) and discuss how the various OFDM parameters affect it. Finally, we will provide a survey of PAR-reduction techniques that have been proposed.

1.1 OFDM System

In an OFDM system, data is modulated in the frequency domain to N adjacent subcarriers. These N subcarriers span a bandwidth of B Hz and are separated by a spacing of $\Delta f = B/N$. The continuous-time baseband representation of this is

$$x(t) = \frac{1}{\sqrt{N}} \sum_{k=0}^{N-1} X[k]\ e^{j2\pi\Delta f k t/T}, \quad t \in [0, T], \tag{1}$$

where $T = 1/\Delta f$ is the symbol period and $\{X[k]\}_{k=0}^{N-1}$ are the data symbols drawn from a finite constellation.

In practice, the baseband modulation is done in the digital domain using an oversampled version of $x(t)$ given by

$$x[n/L] = \frac{1}{\sqrt{LN}} \sum_{k=0}^{N-1} X[k]\ e^{\frac{j2\pi kn}{NL}} \quad n \in [0, NL-1], \tag{2}$$

where L is the oversampling factor. Notice that when $L = 1$ $x[n]$ is the Nyquist-sampled version of $x(t)$. For notational convenience, define column vectors $\boldsymbol{x}_L = \{x[n/L]\}_{n=0}^{NL-1}$ and $\boldsymbol{X} = \{X[k]\}_{k=0}^{N-1}$.

In order to avoid inter-symbol interference (ISI), OFDM systems append a cyclic prefix (CP) to the time domain signal. The length of the CP is set to be at least the maximum delay spread, N_τ, of the channels response, $\{h[n]\}_{n=0}^{N_\tau-1}$, where $h[N_\tau - 1] \neq 0$. The CP can be thought of as a buffer that shields the symbol of interest from being corrupted by reflected versions of the previous symbol. A Nyquist-sampled OFDM symbol with a CP is define by $\{x_{\text{cp}}[n]\}_{n=-N_\tau}^{N-1}$ where

$$x_{\text{cp}}[n] = x[N+n], \quad n \in [-N_\tau, -1] \tag{3}$$

$$x_{\text{cp}}[n] = x[n], \quad n \in [0, N-1]. \tag{4}$$

Using a CP in OFDM simplifies the receiver equalization considerably. First of all, it allows OFDM symbols to be equalized one symbol at a time. Secondly, if the delay profile is constant over the entire symbol period, then

$$y[n] = x_{\text{cp}}[n] * h[n], \quad n \in [-N_\tau, N + N_\tau - 2] \tag{5}$$

$$y_{\text{nocp}}[n] = y[n], \quad n \in [0, N-1] \tag{6}$$

$$= x[n] \ (*)_N \ h[n], \tag{7}$$

where $(*)_N$ is the N length circular convolution. It is well know from DSP theory that $FFT\{x[n] \ (*)_N \ h[n]\} = H[k]X[k]$. Thus, if the channel response is known, the receiver can generate

$$X[k] = FFT\{y_{\text{nocp}}[n]\}/H[k] \tag{8}$$

to recover the data. Figure 1 is a block diagram of an OFDM system. The serial input bit stream is sent to a constellation encoder which outputs N parallel constellations point representing the data. The IFFT of these N samples is used to create the OFDM discrete-time symbol. The parallel time-domain samples are then converted to a serial stream and the CP is added. next the sequence is upsampled, filter, converter to an analog signal, up converted to the carrier frequency, amplified and transmitted. The received chain a mirror image of the transmit chain except that the received frequency domain data is equalized according to (8).

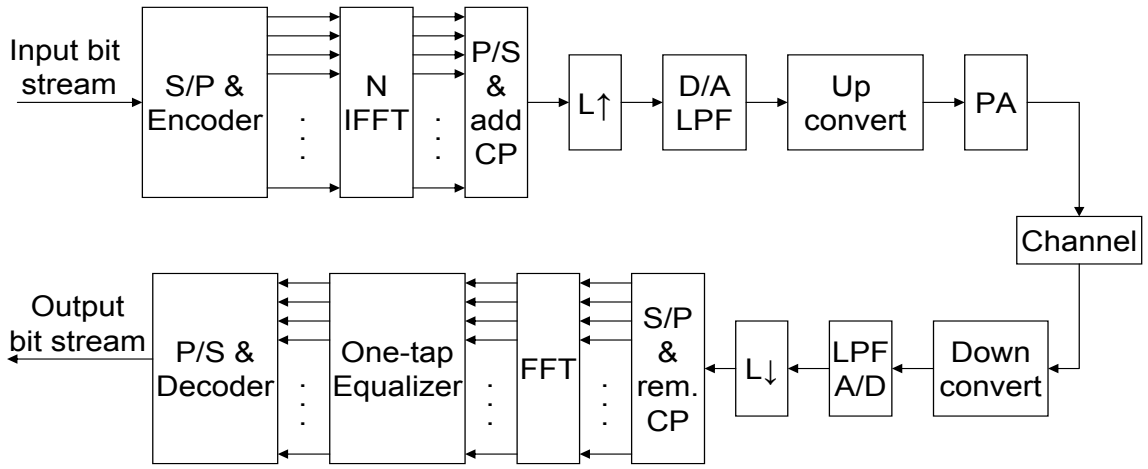

Figure 1: OFDM block diagram.

1.2 Envelope Variation Metrics

As was mentioned in the introduction, the power efficiency of a system suffers when signal that have large envelope variations are used. There have been several metrics proposed that quantify peaky behavior. One such metric is the power variance, ν_e^2, defined in [13] by

$$\nu_e^2 = \frac{E\left[|x|^4\right]}{E\left[|x|^2\right]^2}, \tag{9}$$

where $E[\cdot]$ denotes the expected value. In [13] the author showed that ν_e^2 is directly proportional to the normalized mean squared error between a second-order nonlinear function of x and a linear function of x. While ν_e^2 is interesting for analysis, it has not proven to be a useful metric for OFDM signals passing through peak-power limited devices.

Figure 2 is a plot of the complementary cumulative distribution function (CCDF) of the envelope power of OFDM. The plot is for $N = 16,\ 256,\ 1024$. From the plot we can see that the CCDF is almost constant. Because the plot is linear-log scale, the linearity of the CCDF implies an exponential distribution. In fact, the large N becomes, the more exponential the line becomes.

Intuitively, using some normalized measurement of the peak of a signal is appealing. This is the idea behind the peak-to-average ratio discussed in the next section. However, recently Lei, Li and Tang pointed out that in practical systems, signals are frequency clipped to some low level even after envelope peaks have been minimized [38]. Accordingly, they

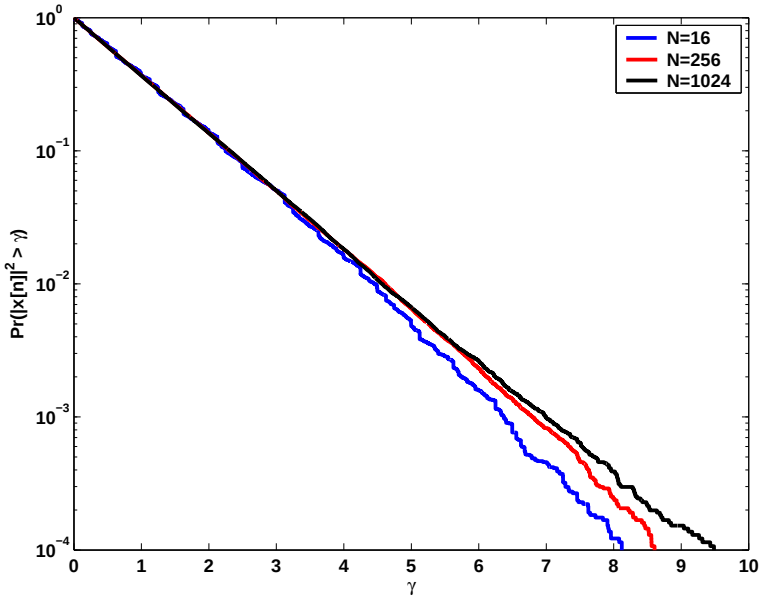

Figure 2: Envelope power CCDF of OFDM for $N = 16,\ 256,\ 1024$.

propose that the envelope variation of a signal be measured by the clipping noise power generated at some clipping level.

1.3 Peak-to-Average Ratio

The most popular quantification metric of envelope variation is the peak-to-average ratio (PAR)[1]. Rightfully so, as PAR captures the most important aspect of a signal that has to pass through a peak-power limited device: the peak power.

The use of PAR in communications signals is a result of the use of PAR in radar applications. A radar system shares certain similarities with a communications system; namely, they both have to transmit an amplified radio signal of a certain spectrum. For radar, the spectrum shape is often the only signal constraint, which makes waveform shaping that minimizes peaks a relatively straightforward problem. However, in an OFDM communication system there is the additional constraint that each subcarrier (Fourier coefficient of the spectrum) is modulated with an information bearing complex number. This additional degree of constraint significantly complicates the problem.

[1]PAR is alternately referred to as the PAPR (peak-to-average power ratio) and PMEPR (peak to mean envelope power ratio). PAR is also directly related to the crest factor (CF) of a signal where $CF = \sqrt{PAR}$.

Define the PAR of an OFDM signal, x to be

$$PAR\{x\} = \frac{\max |x|^2}{E\left[|x|^2\right]}, \tag{10}$$

where x and be any signal representation (critically sampled baseband, oversampled baseband, continuous-time passband, etc.) defined over one symbol period. Because the denominator of (10) is an expected value and, strictly speaking, not an "average," it is true that the term PAR is a bit of a misnomer. Despite this slight technical inaccuracy, PAR is the most widely used term and we will keep with convention here. Also, note that the ensemble average power and the expectation in the denominator of (10) only differs for non-constant modulus constellations. Figure 3 is a plot of the PAR of $x[n]$ for different N. It is obvious that at all probability levels the PAR increases with N

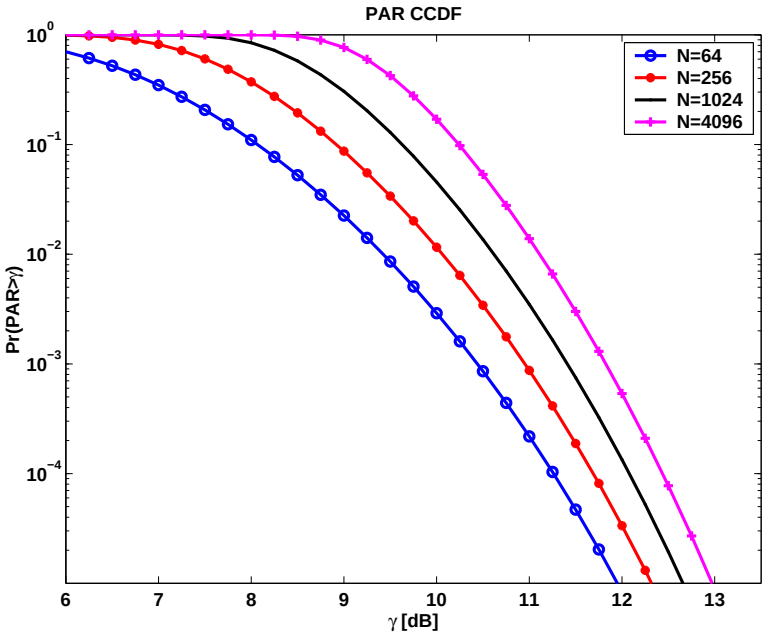

Figure 3: CCDF of the discrete-time PAR for various values of N.

In the discrete-time case, where only the Nyquist sampled analog signal is examined, the cumulative distribution function (CDF) can be easily derived if certain assumptions are made. First we assume that N, the number of subcarriers, is large enough so that the discrete-time domain signal has an approximate complex Gaussian distribution [15]. It then follows that the instantaneous power of the discrete-time domain samples is Chi-Squared distributed. Therefore, for a given $n = n_o$, $|x[n_o]|^2$ is χ^2 distributed with two degrees of

freedom. So $Pr[|x[n_o]|^2 < \gamma] = 1 - e^{-\sigma_x^2 \gamma}$. Furthermore, according to Theorem 4.4.1 of [15], after the IFFT each discrete time sample can be treated as independent of all other samples. With these two approximations, the probability that the power of at least one $x[n]$ out of N samples is above a given level, γ, is

$$\Pr\left[\max_{0 \le n < N} |x[n]|^2 < \gamma\right] = (1 - e^{-\sigma_x^2 \gamma})^N. \tag{11}$$

Finally, if $E\left[|x[n]|^2\right]$ is normalized to unity, then the CCDF of the PAR is

$$\Pr\left[PAR\{x[n]\} > \gamma\right] = 1 - (1 - e^{-\gamma})^N. \tag{12}$$

It is natural to wonder what PAR is of the most interest in an OFDM system. For instance, when an engineer has to specify the dynamic range of the digital-to-analog converter (DAC) in an OFDM system, the most important PAR measurement would be that of the signal input to the DAC which is $x[n/L]$. On the other hand, the PA will have to be designed around the PAR of the passband signal $x_{pb}(t) = \Re\{x(t)\ e^{j2\pi f_c t}\}$, where f_c is the carrier frequency. If $f_c >> B$, which is the case in most practical systems, then

$$\max|x_{pb}(t)| \approx \max|x(t)|. \tag{13}$$

Also,

$$E\left[|x_{pb}(t)|^2\right] = E\left[|\Re\{x(t)\ e^{j2\pi f_c t}\}|^2\right] \tag{14}$$

$$= E\left[\Re\{x(t)\}^2\ \cos^2(2\pi f_c t) + \Im\{x(t)\}^2\ \sin^2(2\pi f_c t)\right] \tag{15}$$

$$= \frac{1}{2} E\left[\Re\{x(t)\}^2 + \Im\{x(t)\}^2\right] \tag{16}$$

$$= \frac{1}{2} E\left[|x(t)|^2\right]; \tag{17}$$

therefore,

$$PAR\left\{x_{pb}(t)\right\} \approx 2\ PAR\left\{x(t)\right\}. \tag{18}$$

Equation 12 is a very good approximation to the PAR distribution of $x[n]$, but differs but as much as one dB from the PAR distribution of $x(t)$. There have been several attempts to determine the distribution of $x(t)$. The first came from [63], where is was claimed that

$$\Pr\left[PAR\{x(t)\} > \gamma\right] \approx 1 - (1 - e^{-\gamma})^{2.8N}, \tag{19}$$

which is just a intuitive modification to the CCDF that resulted from the Gaussian approximation in (12). Later in [23], a more theoretical analysis of the problem was done based on level crossing probabilities of $x_{pb}(t)$, where the ratio f_c/B was taken into account as well as the power distribution of $X[k]$. They concluded that for $f_c >> B$ and a constant modulus power distribution that

$$\Pr\left[PAR\{x(t)\} > \gamma\right] \leq N\sqrt{\frac{\pi}{3}\gamma}e^{-\gamma}. \tag{20}$$

In [45], the authors present the approximation

$$\Pr\left[PAR\{x(t)\} > \gamma\right] \approx \begin{cases} \left(1 - \frac{\sqrt{\gamma}e^{-\gamma}}{\sqrt{\bar{r}}e^{-\bar{r}}}\right)^{N\sqrt{\frac{\pi}{3}\bar{r}}e^{-\bar{r}}}, & \gamma > \bar{r}; \\ 0, & \gamma \leq \bar{r}, \end{cases} \tag{21}$$

where $\bar{r} = \sqrt{\pi}$, based on the level crossing rates of $x(t)$. The authors further refine (21) for large γ to

$$\Pr\left[PAR\{x(t)\} > \gamma\right] \approx e^{N\sqrt{\frac{\pi}{3}\gamma}e^{-\gamma}}. \tag{22}$$

In order to test these approximations it is necessary to resort to digital signal theory where it is known that as $L \to \infty$, $x[n/L] \to x(t)$. It follows that the PAR of $x[n/L]$ approaches the PAR of $x(t)$ for large L. Thus we should be able to approximate $PAR\{x(t)\}$ by running simulations on the oversampled signal $x[n/L]$.

Figure 4 is a plot of each approximation to the PAR of $x(t)$ as well as the PAR of $x[n/L]$ for $L \in \{1, 2, 4, 8\}$. From the plot we can see that the oversampled PAR is only slightly larger than the Nyquist-sampled PAR. Additionally, the PAR for $L = 4$ is very close to the $L = 8$ case, which is indistinguishable from larger Ls (not plotted). The approximations to the continuous-time PAR are fairly tight, but they all appear to be upper bounds.

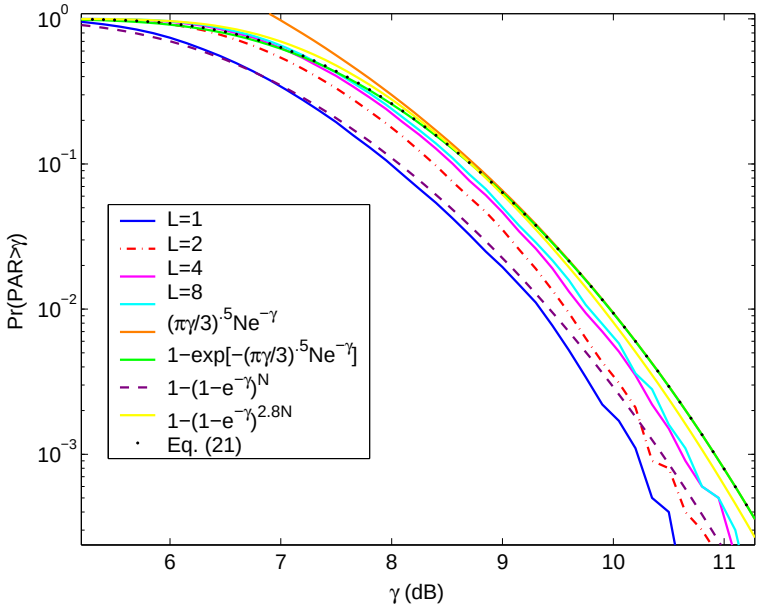

Figure 4: CCDF of the PAR for $L \in \{1, 2, 4, 8\}$, $N = 64$ and the approximations in (12), (19), (20), (21) and (22).

1.4 Conclusions

In this chapter we summarized the history of OFDM and demonstrated that it is a popular communications technique. Despite its popularity, it suffers from large envelope variations. Accordingly, we presented several envelope variation metrics and provided a thorough analysis of the most popular metric: the peak-to-average ratio.

CHAPTER II

PAR REDUCTION

From Chapter 1, we know that OFDM is a promising high-speed communications technique. However, it suffers from high PARs. In this chapter we will give an overview of PAR reduction, including a survey of various PAR reduction techniques that have been presented in the literature.

2.1 Early Applications

PAR reduction was first of interest for radar and speech synthesis applications. In radar, PAR reduction was important because radar systems are peak-power limited just like communications systems. In speech synthesis applications, peaky signals lead to a hard sounding "computer" voice [57]. In simulating human speech this characteristic is not desirable[1]. However, in both radar and speech synthesis, maintaining a certain spectral shape is of interest. Therefore, PAR reductions in these fields can be done per spectral shape and are specified by frequency-domain phase sequences. Some examples of low-PAR sequences are the Newmann phase sequence, the Rudin-Shapiro phase sequences, and Galios phase sequences. These phase sequences all produce low PAR time-domain sequences for a wide variety of spectral masks. But this is not sufficient for OFDM where *random* data is modulated in the frequency domain. As a matter of fact, it is impossible to find a phase sequence that produces a globally low PAR for all data sequences.

Another difference between communications PAR reduction and radar of speech PAR reduction is that communications systems, out of necessity, must occasionally distort or clip signals that exceed some peak threshold. Because some sort of distortion will occur, communications PAR reduction scheme are not limited to being distortionless.

[1]It is intriguing that the human body has also addressed the PAR reduction problem in the sense that human speech is not as peaky as it could be given the audible spectrum.

2.2 Distortion Techniques

It is difficult to precisely sort PAR reduction schemes into distortion and distortionless categories. Here, we consider schemes that introduce spectral regrowth to be distortion techniques. Distortion techniques are the most straightforward PAR reduction methods. In general, they do not require any side information to be sent which mean the data rate is unchanged even after PAR reduction and they have low complexities compared to the distortionless techniques. However, the price paid for using a distortion technique is distortion noise which adversely affects the error rate of the system. Furthermore, these techniques distort the spectrum, which makes conforming to regulatory spectral masks difficult. This spectrum distortion or "spectral regrowth" can be corrected by filtering, but the filtering will likely regrow the peaks that were originally reduced. The problem can be thought of as trying to plug two holes with only one plug. That is, the PAR can be reduced at the expense of spectral regrowth or the spectral regrowth can be reduced at the expense of PAR.

2.2.1 Clipping

The simplest distortion technique is clipping, where peaks above a certain threshold, γ_o, are "clipped" back down to the threshold according to

$$\tilde{x}(t) = \begin{cases} x(t), & |x(t)| \leq \gamma_o; \\ \gamma_o e^{j\angle x(t)}, & |x(t)| > \gamma_o, \end{cases} \tag{23}$$

If the clipping is too hard (i.e. γ_o is too small), then significant spectral regrowth will occur. This phenomenon can be observed in Figure 5 and is treated theoretically in [48]. In addition to spectral regrowth, clipping an OFDM signal also introduces clipping noise which increases error rates. While it is not strictly accurate, clipping noise can be thought of as approximately independent additive gaussian noise [46][68], which leads to a simple SER expression in AWGN channels. Define the signal to noise plus distortion ratio (SNDR) as

$$SNDR = \frac{\sigma_x^2}{\sigma_N^2 + \sigma_C^2}. \tag{24}$$

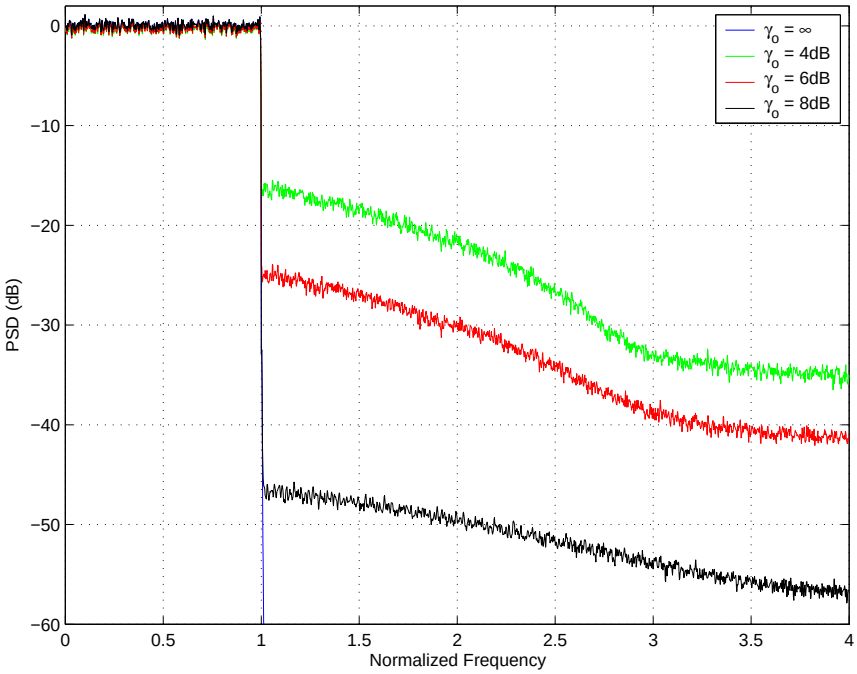

Figure 5: Power spectral density of clipped OFDM symbols where $N = 1024$. The unclipped case is presented along with clipping levels of $\{4,\ 6,\ 8\}$ dB ($\sigma_x^2 = 1$).

The expected clipping noise power can be approximated as the tail expectation of a χ^2 distribution for large N because $x[n] \sim$ C.G.$(0,\sigma_x^2)$ or

$$\sigma_C^2 = \frac{1}{\sigma_x^2} \int_{\sigma_x^2\gamma_o^2}^{\infty} \gamma e^{-\gamma/\sigma_x^2}\, d\gamma \tag{25}$$

$$= \frac{(1+\sigma_x^2\gamma_o^2)e^{-\sigma_x^2\gamma_o^2}}{\sigma_x^4}. \tag{26}$$

The symbol error rate (SER) for a QAM constellation for a clipped symbol in an AWGN channel can be approximated by [51]

$$SER = 1 - \left[1 - 2\left(1 - \frac{1}{\sqrt{M}}\right) \mathrm{Q}\left(\sqrt{\frac{3SNDR}{M-1}}\right)\right]^2, \tag{27}$$

where $\mathrm{Q}(\cdot)$ is the tail area of the normal distribution. Figure 6 is a plot of the symbol error rate (SER) for different clipping levels. From the plot we can see that light clipping results in only small increases in error rate.

It may initially be perplexing to think that the expected clipping noise power (and the SER) are independent of N. Actually, it is not independent of N. From (26), the clipping noise power depends on σ_x^2, which is a function of N. However, this is still not completely

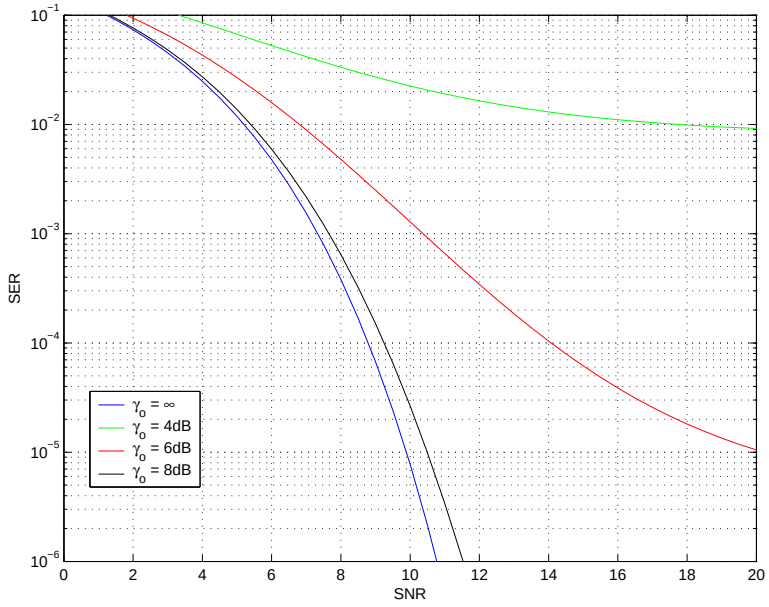

Figure 6: Approximate symbol error rate of clipped OFDM symbols for large N and $M = 4$. The unclipped case is presented along with clipping levels of $\{4,\ 6,\ 8\}$ dB ($\sigma_x^2 = 1$).

settling because it means that the normalized clipping power is independent of N. One may look back and see that the PAR, which is also normalized by σ_x^2 grows with N (we will show later that it is unbounded growth), which would seem to infer that the clipping power would grow with N as well. But this is not the case. Remember that the PAR is a measurement of the maximum peak (a rank statistic), whereas clipping noise power depends on the probability density above the clipping level. The former increases with N, while the latter is unaffected by N (according to our approximation).

It is common to see error-rate plots of PAR reduced signals, but rarely is any attempt made to include the positive affects of the PAR decreases in the plot. We advocate plotting the SER or BER versus the peak signal-to-noise power ratio (PSNR) so that the peak reduction is taken into account. In Figure 7 the SER is plotted versus PSNR and we can see that from this perspective 8dB clipping outperforms 10dB clipping.

There have been several proposals that aim at mitigating the spectral regrowth and SER increases due to clipping. Notably, Kim and Stuber in [36] present an iterative receiver design that tries to undo the clipping effect to increase the SER. The procedure is to take the received clipped signal, $\tilde{x}[n]$ and map it to constellation points so that $\hat{X}[k]$ is generated.

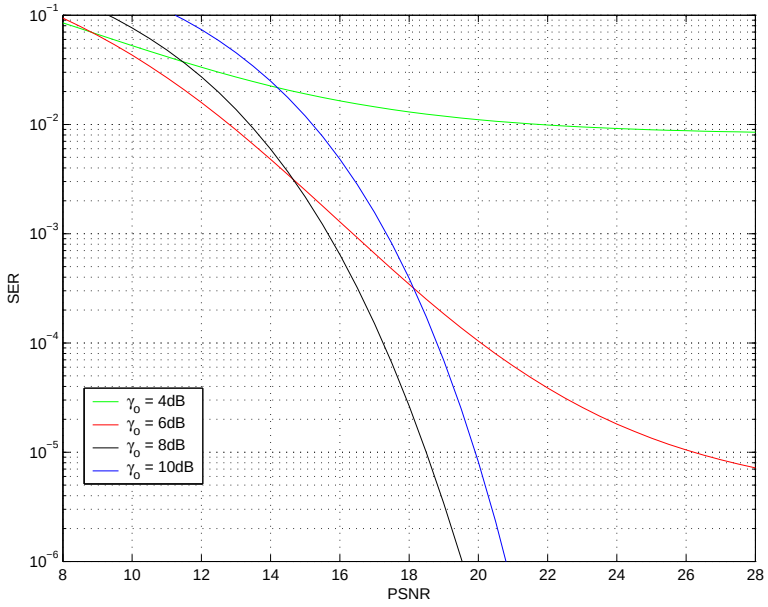

Figure 7: Approximate symbol error rate presented versus the *peak* signal to noise power ratio of clipped OFDM symbols for large N and $M = 4$.

Then, find $IDFT\{\hat{X}[k]\} = y[n]$, which is used to estimate the unclipped signal

$$\hat{x}[n] = \begin{cases} \tilde{x}[n], & |y[n]| \leq \gamma_o; \\ y[n], & |y[n]| > \gamma_o. \end{cases} \tag{28}$$

This technique was dubbed decision aided reconstruction (DAR) by the authors. A very similar method is detailed in [60] called the iterative quasi-ML nonlinear distortion canceller.

2.2.2 Companding

Another distortion technique is companding. Companding is a composite word that combines **com**press and ex**pand**. It was first used as a technique to expand the dynamic range of DACs [35] and was later adopted as a perspective PAR reduction technique [65]. The basic idea is to employ a compressing function, $\mathrm{F}(\cdot)$, in the transmitter and apply it to the OFDM symbol x so that $\mathrm{F}(x)$ is transmitted, where the range of $\mathrm{F}(x)$ is less than the range of x. Three example companding functions are plotted in Figure 8. In the receiver, the expanding function $\mathrm{F}^{-1}(\cdot)$ is applied to the received symbol y so that $\hat{x} = \mathrm{F}^{-1}(y)$ approximates the original symbol. The drawback to companding is that when the received symbol is expanded, so is any distortion from the channel, which means detection rates are degraded. Also, there will be spectral regrowth in the compressed signal.

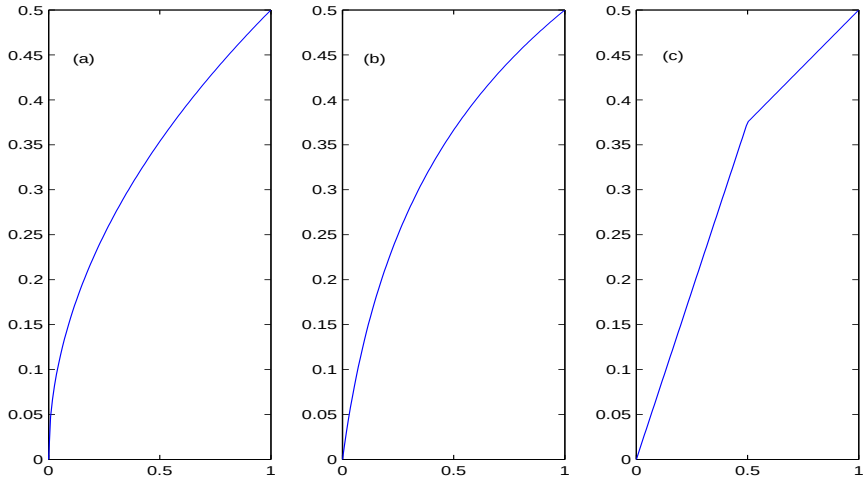

Figure 8: Three compressing functions. (a) is square root function, (b) is the μ-law function [65] and (c) is a piece-wise linear function.

2.3 Distortionless Techniques

In this section we introduce distortionless PAR-reduction techniques. While none of these reduction techniques introduce spectral regrowth, some of them do introduce additional noise to the system thereby increasing the error rate. Other techniques require overhead information bits to be sent along with the transmitted signal so that the receiver can reverse the PAR reduction transformation and recover the data. This has the negative effect of decreasing the useful data throughput.

2.3.1 Average-Power-Preserving Techniques

In an average-power-preserving technique, high PAR signals are mapped to low PAR signals by rearranging the constellation points in a reverable way such that the average power of the signal is not increased. In general, average power increases are detrimental to system performance.

One could reasonably argue that requiring the transmission of side-information increases the average signal power compared to the unreduced signal, but a semantic line has to be drawn somewhere. So, for our purposes, techniques requiring side information that do not otherwise increase the average power of a signal are considered average-power preserving.

2.3.1.1 Systematic Coding

Systematic coding PAR reduction techniques are based on the idea that there are a finite number of low-PAR OFDM symbols. This number is obviously less than the number of possible OFDM symbols. So with a data rate reduction, it is possible to "code" data sequences to low-PAR sequences. The first attempt at this method was made by Popovic in [50] where is was suggested to use binary Golay codes as frequency domain symbols. Golay codes were already known to have low PARs [44], so the choice was natural. However, the problem is that OFDM using QAM should be able to transmit 4^N different sequence, however, there are only N^c, where c depend on N, unique binary golay sequences, thus the coding rate would become impractically small for even small N.

A different approach to applying coding to PAR reduction was taken in [33]. There it was suggested that an exhaustive search could be done over all the possible bit combinations in order to find a set with acceptably low PAR. The problem is that the search space grows exponentially with N (as does the memory required to store the code), so this technique is not useful for large N either.

2.3.1.2 Selective Coding

Selective coding is a broad classification, which falls under the even broader class of PAR reduction techniques that randomly create alternate symbol mappings to generate low-PAR symbols. The distinction is that selected coding techniques implement some sort of coding method to determine which mapping is used, and possibly, to recover corrupted data bits.

A data vector scrambling method was proposed in [14]. In the method scrambling (interleaving) is preformed with a feedback shift register, such that different feedback patterns were used to create independent mappings. For the receiver to detect how the data was scrambled, a prefix label of several subcarriers must be inserted in the frequency domain by the transmitter before scrambling. In the receiver, the possible feedback patterns are tested and the one that most accurately restores the label is used.

In [16] the feedback idea was extended. The authors of that paper proposed that a repeat accumulate code be used before the feedback register. Thus, the receiver could use a

MAP decoder to determine the initial state of feedback register for the PAR reduced signal without having to insert a prefix label.

More recently, in [62] an erasure coding method combined with PAR reduction was proposed. In that method, the data from one OFDM symbol is block coded. After the block code, redundancy has been introduced. Thus, they propose to use different erasure patterns to generate OFDM symbols and select the one with the lowest PAR. Because the data has been coded, it can still be recovered; however, the recovery is sensitive to the structure of the erasure pattern. This method is interesting, but achieves only limited PAR reduction because each of the erased candidate signals are highly correlated.

A PAR-reduction method that used a turbo coding scheme was presented in [4]. In that scheme all combinations of a prefix of B bits are concatenated to the data vector before turbo coding to create a number of candidate bit sequences. After the turbo encoder, each of the 2^B prefix bit combinations will create an approximately independent mapping. The mapping with lowest PAR is selected for transmission. In the receiver, a turbo decoder is used and the the prefix bits are simply discarded, as they carry no information. This scheme can also be applied to low density parity check (LDPC) codes, that, like turbo codes, create approximately independent output sequences even for high correlated input sequences. The problem with these methods is that the complexity is very high and inserting bits before encoding is expensive in terms of data rate sacrifice.

2.3.1.3 Partial Transmit Sequence

Partial Transmit Sequence (PTS) was introduced in [42] as a PAR reduction scheme. In PTS, the frequency domain symbols, $\boldsymbol{X}$, get partitioned into D disjoint blocks, $\{\boldsymbol{X}^{(d)}\}_{d=0}^{D-1}$ that are zero-padded to be length N so that

$$\boldsymbol{X} = \sum_{d=0}^{D-1} \boldsymbol{X}^{(d)}. \tag{29}$$

The end goal is to multiply each block by an optimized sequence of phase constants $\{e^{j\phi^{(d)}}\}_{d=0}^{D-1}$, such that the PAR is reduced. It is assumed that the constants are drawn from a finite set $\mathcal{A}$, where $|\mathcal{A}| = P$. The beauty of PTS is that this can be done in the time

domain because the IDFT is linear. That is,

$$IDFT\left\{\sum_{d=0}^{D-1}\boldsymbol{X}^{(d)}e^{j\phi^{(d)}}\right\}=\sum_{d=0}^{D-1}IDFT\left\{\boldsymbol{X}^{(d)}\right\}e^{j\phi^{(d)}}. \tag{30}$$

Therefore, the PAR can be checked without having to go back and forth between the time and frequency domains (as is the case with SLM). Stated concisely, the goal of PTS is to find $\{e^{j\phi^{(d)}}\}_{d=0}^{D-1}$ according to

$$\{\phi^{(d)}\}_{d=0}^{D-1}=\underset{\{\phi^{(d)}\}_{d=0}^{D-1}}{\arg\min}\left[\max\left|\sum_{d=0}^{D-1}IDFT\left\{\boldsymbol{X}^{(d)}\right\}e^{j\phi^{(d)}}\right|\right]. \tag{31}$$

PTS can be quite effective at reducing the PAR; however, the PAR reduction capability depends on the size of D and P. Effectively, there P^D "mappings" in a PTS scheme at the cost of D IFFT operations[2]. But, as we will discuss in the next chapter, the mappings are not even approximately independent, thus, the PAR of one mapping is correlated with the PAR of another mapping. In terms of PAR reduction capability, this means that PTS falls well short of a scheme (like SLM) that tests P^D *independent* signal mappings.

Another difficulty for PTS is that side information that can distinguish P^D different mappings must be transmitted, which can take up to $D\log_2 P$ bits. There have been several proposed PTS side information schemes [31] [25] and all of the SLM blind detection methods that we discuss in this thesis are also applicable. But there is still a sub-optimal element to PTS where more mappings than necessary are being tried per PAR reduction which leads to more side information than necessary being transmitted per PAR reduction. A third difficultly in PTS is solving (31). One method is to randomly search the possible combinations. And there have been several attempts at more elegant solutions [34][28][20]. But all of these methods increase the complexity of the system by some unspecified amount making a PAR-to-complexity tradeoff analysis difficult.

In the next chapter we will discuss selected mapping (SLM) which is also an alternative mapping technique. In fact, PTS and SLM are both generalizations of each other. That is, SLM is PTS where, instead of blocks of subcarriers being rotated, each subcarrier is rotated individually.

[2]These D IFFT operations are on mostly zero sequences, thus the complexity is not $\mathcal{O}(DN\log N)$. Instead it is $\mathcal{O}(DN\log\frac{N}{D})$ [64].

2.3.2 Average-Power-Increasing Technique

Initially, it is intuitive to think that increasing the average power is a good thing, and it may be if the increase goes towards enlarging the minimum distance between constellation points. In that case the error rate will be decreased. However, all of these methods increase the average power *without* changing the minimum distance of the constellation. The problem with this is illustrated in Figure 9, where a peak-power constraint of 4W is assumed. In the top of the figure is a process for a average-power-preserving PAR technique. There, the "scale signal" block does not actually to do anything because the constraint has already been met. On the other hand, for the average-power-increasing technique, after the PAR reduction is done, the average power has increased. Since the PAR is a ratio of peak to average power, the PAR contains only relative information about the peak power. In a peak-power constraint system, the absolute peak power is of interest. The example in Figure 9 demonstrates an average power increase of 10%, which, which after the peak is scaled to meet the peak-power constraint means the effective signal power is $\frac{1}{1.1} = 90.9\%$ of the effective signal power of a signal passing through a average-power-preserving reduction technique. Small increases in average power may not be significant, but be wary of perspective PAR-reduction schemes that promise large PAR reductions at the cost of decreased minimum distances. Interestingly, none of the papers in this area has examined the point of diminishing return in the algorithms. That is, at what point does the average power increase outpace the PAR reduction?

Another consideration with the power increasing systems is sidelobe enlargement. Basically, the power increase has to be placed somewhere in the bandwidth of the OFDM system. If too much extra energy is placed in subcarriers at the edge of the OFDM bandwidth, then the sidelobes will become larger and the system may no longer meet regulatory spectral masks.

2.3.2.1 Tone Reservation

The idea behind tone reservation is to isolate energy used to cancel large peaks to a predefined set of tones. These tones do not bear any useful information and are orthogonal

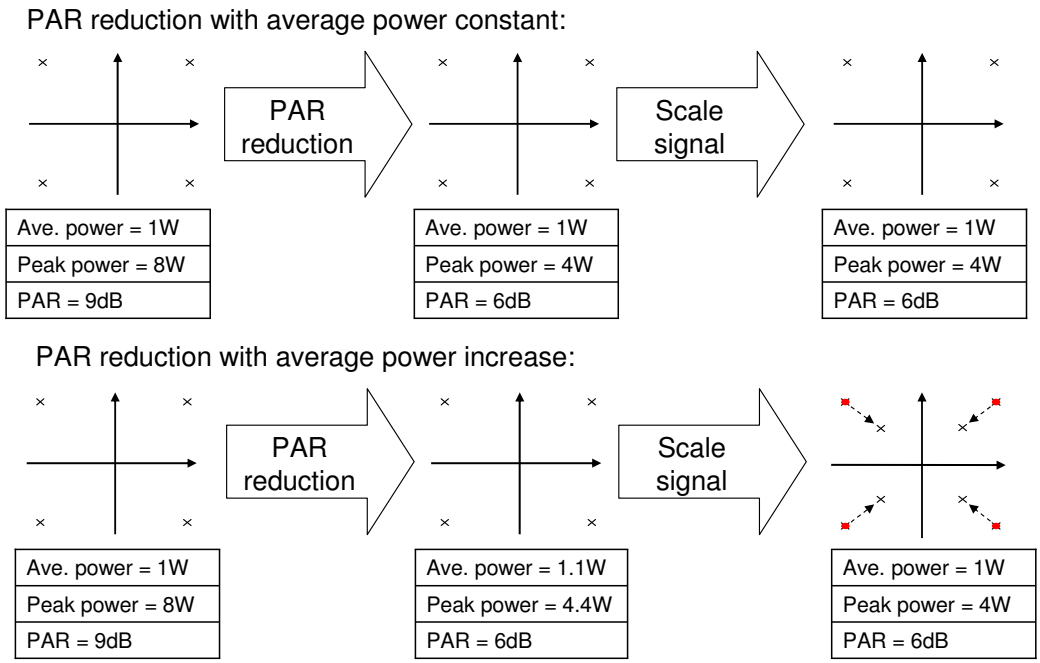

Figure 9: Illustration of the disadvantage of average power increasing PAR reduction methods.

to the data bearing tones. This orthogonality makes recovering the data trivial. Stated mathematically, the transmitted signal is

$$\tilde{x}[n/L] = x[n/L] + \tilde{c}[n/L], \tag{32}$$

where $c[n/L]$ is the signal used to cancel large peaks. The indices of the tones reserved for PAR reduction belong to $\mathcal{B}$. In the frequency domain,

$$\tilde{X}[k] = \begin{cases} X[k], & k \in \mathcal{B}^{\perp}; \\ \tilde{C}[k], & k \in \mathcal{B}. \end{cases} \tag{33}$$

In tone reservation the optimal values for the reserved tones are given by

$$\tilde{C}[k] = \underset{C[k]}{\arg} \min_{k \in \mathcal{B}} \left[\max \left| x[n/L] + IDFT_L\{C[k]\} \right|^2 \right]. \tag{34}$$

While the problem is simple to explain, the solution is difficult. However, because it is a minimization over convex (quadratic) constraints, it is solvable. Moreover, there is a large amount of material on quadratically constrained problems [27].

Tone reservation was first introduced in [26]. In that paper, the authors implemented a projection onto convex sets (POCS) method for solving (34). POCS is an active field with

many applications like filter design, array signal processing, electron microscopy, speckle interferometry, topography, spectral estimation, neural networks [21], and PAR reduction. Basically, the idea is to find an element that exists in two sets. In POCS the element is found through iterative projections from one set to the next. In the context of PAR reduction, these two sets are $x[n/L]$ with a peak below a certain threshold and a $C[k]$ that is nonzero only when $k \in \mathcal{B}$. Practically, this is accomplished by the following steps

1. Clip $x[n/L]$ to generate $x[n/L] - \hat{c}[N/L]$.
2. Compute $DFT\{\hat{c}[N/L]\} = \hat{C}[k]$.
3. For $k \notin \mathcal{B}$ set $\hat{C}[k] = 0$.
4. Compute $x[n/L] = IDFT_L\{X[k] + \hat{C}[k]\}$.
5. If max $|x[n/L]|$ is below threshold, quit. Otherwise goto step 1.

Later, Tellado and Cioffi discussed the idea of tone reservation [61] [60]. They provided a detailed analysis of how to solve (34) as a linear programming problem that has an exact solution (the POCS method is suboptimal). The linear programming solution can be reached with complexity $\mathcal{O}[N \log N]$. They also detailed a (suboptimal) gradient search method in [60] with complexity $\mathcal{O}[N]$.

While promising, tone reservation has serval shortcomings. First is that data rate is necessarily decreased because some tone are used strictly for PAR reduction. In some static channels this is an acceptable condition because some subcarriers are known to have such a low SNR that no information would be transmitted on them anyway. The second problem is the difficulty of selecting which tones to reserve. This problem has not been well-studied, but the choice of tones is known to have a large affect on the PAR reduction capability. A random search over all the possible sets, $\mathcal{B}$, would greatly increase the complexity of tone reservation. Often the tones have to be chosen contiguously because fades often affect contiguous sets of subcarriers. These contiguous sets of tones are known to have bad PAR reduction abilities. The third issue is a tradeoff between the number of reserved tones and the average power increase due to tone reservation. The more tones that are reserved the

less power needs to be allocated to PAR reduction. On other hand, more reserved tones mean more unused bandwidth that could be data bearing.

2.3.2.2 Tone Injection

Motivated by the data rate loss of tone reservation, Tellado introduced tone injection [60]. In tone injection, the constellation is enlarged to include S times as many points as the original constellation. The extra constellation points are generated by shifting copies of the original constellation. Figure 10 illustrates the possible positions for a QSPK constellation for tone injection when $S = 9$. That is, there are 8 alternative representations for each constellation point. If necessary, S could be made larger by extending the replication pattern over more of the signal plane. The constellations are separated by distance p where for an M-QAM constellation $p \geq d_{\min} \log_2 M$ so that $d_{\min}$ for the extended constellation is the same as the original $d_{\min}$.

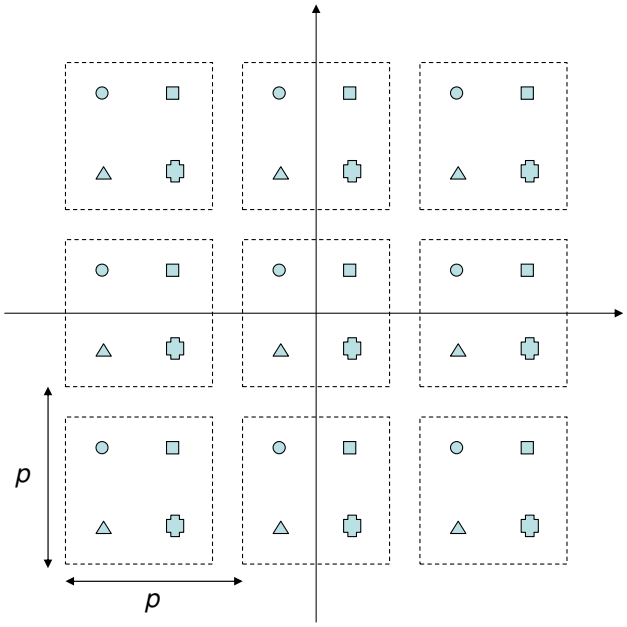

Figure 10: QPSK constellation extended for tone injection ($S = 8$).

Tone injection works by moving constellation points from the original constellation to one of its corresponding points in the extended constellation. If done properly, this rearrangement will lead to a PAR reduction. The clever trick is that the receiver can recover which constellation point an received extended point corresponds to by taking the modulo

Table 1: Maximum PAR reduction in 64QAM with $N = 64$. The original PAR is assumed to be 15dB (10^{-7}). Reproduced from [60]

B	$\rho = 1$	$\rho = 1.125$	$\rho = 1.25$
1	1 dB	1.1 dB	1.3 dB
2	2.2 dB	2.5 dB	2.8 dB
3	3.5 dB	4 dB	4.6 dB
4	5 dB	6 dB	7 dB

p of the in-phase and quadrature-phase components of the received signal. Thus, no side information is necessary to recover the original signal from the PAR reduced signal. However, it is obvious that any extension of the constellation will increase the average power.

There are two degrees of freedom in tone injection. The first is, which tones are allowed to be extended. The second is, how much extension is allowed (how large S can be). If the indices of the extended tones are in the set $\mathcal{B}$ and $|\mathcal{B}| = B$ then there are $\binom{N}{B}S^B$ possible combinations, which is a prohibitively large space to search randomly. But a POCS algorithm can be implemented in tone injection as it was described for tone reservation. The only difference is that the projection points in the frequency domain are constrained to one of S points instead of being able to take on any complex value. This method does not have good PAR reduction capability and the complexity can get very large. In [60] presented a maximum PAR reduction analysis where it was assumed that at best the peak power could be reduced by power used in constellation extension. This assumption is very optimistic because in reality, only a fraction of the increase power will go to peak reduction. In some cases a reduction of one peak could lead to another larger peak elsewhere. Table 1 is a reproduction of the results from [60]. In the table ρ is define as

$$\rho = \frac{p}{d_{\min} \log_2 M} \tag{35}$$

and is a measurement of the spacing between shifted constellations. The larger ρ is, the more the average power will increase.

2.3.2.3 Active Constellation Extension

Active Constellation Extension (ACE) was proposed in [37] as a PAR reduction technique. It is similar to tone injection in that an extended constellation is used to cancel time domain peaks. The difference is in how the constellation is extended. Figure 11 illustrate the regions that constellations points can be extended. Notice that, like tone injection, ACE does not explicitly decrease the minimum distance (though, effectively, it does under a peak power constraint system). That is, the constellation points are only allowed in regions of the signal plane that are further from any other points. In order to find the extension points, the same methods used for tone reservation can be employed. Which is either POCS or a gradient search algorithm.

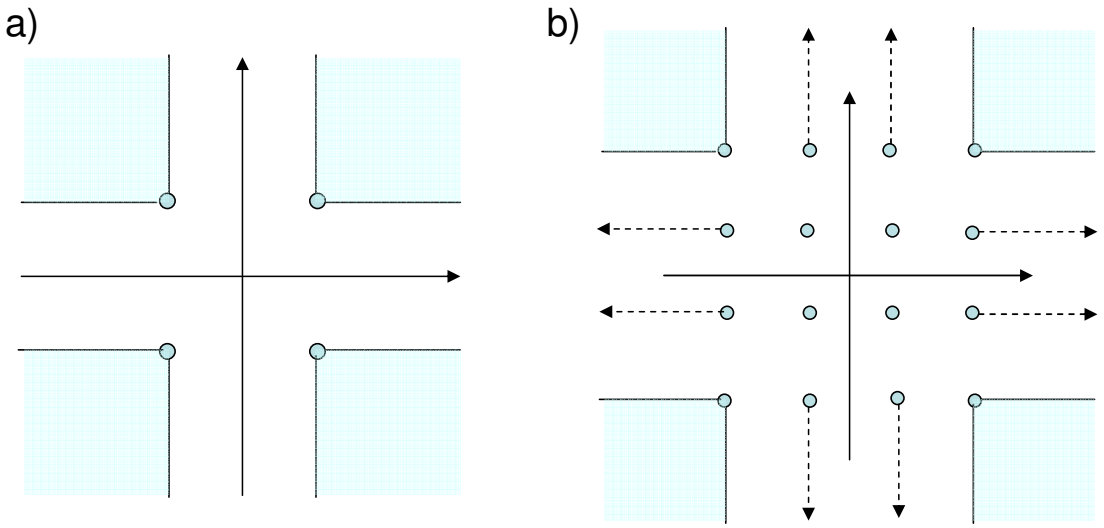

Figure 11: Constellation extensions possible in ACE. Plot a) is for QPSK and b) is for 16-QAM.

2.4 Conclusions

In this chapter we provided an overview of the different PAR reduction techniques. All of these techniques can be though of as a mapping from one signal representation to another that has a lower PAR. For the distortion techniques this mapping causes information to be lost when the mapping is reversed. For some of the distortionless techniques, the mappings were a result of a deterministic solution (e.g. Tellado's tone reservation [60] and some of the

coding techniques [50][33][44]). Others generated mappings according to some structured search (gradient, POCS) so that each successive mapping was guaranteed to have a lower PAR than the mapping from a previous iteration (e.g. tone reservation [26], tone injection [60], ACE [37] and some forms of PTS [34][28][20]). Finally, the last group of distortionless methods randomly searched over a set of candidate mappings to select for PAR (SLM [7], selected coding techniques [62], some forms of PTS [42], and Jayalath's interleaving technique [29]). This type of random searching PAR reduction method was studied in the general form in [32].

CHAPTER III

SELECTED MAPPING

Selected mapping (SLM) is a specific scheme for PAR reduction that was introduced in [7]. But, the idea of mapping a signal to different, but equivalent, signal representations is very general and has been applied in several different forms for OFDM.

One such scheme was detailed in [38], where a method based on selected clipping was introduced. The idea was to create different signal representations of an OFDM symbol, but instead of selection being based on PAR, their scheme selects based on the amount of clipping noise a signal would generated for a given clipping level.

Another selection scheme was presented in [56] that selects OFDM symbols based on the amount of maximum amount of inter-carrier interference (ICI) they may create. This sounds curious at first because we know that ICI is created from carrier offsets in the receiver. But in [56], the authors showed that SLM could be used to minimize the maximum peak interference-to-carrier ratio (PICR) in the receiver, where PICR is a measure of the worst-case ICI.

3.1 Selected Mapping for PAR Reduction

The paper that coined the term "selected mapping" was written by Bauml, Fischer and Huber in 1996 [7]. However, similar ideas were published at almost the same time in [40] and [24]. SLM takes advantage of the fact that the PAR of an OFDM signal is very sensitive to phase shifts in the frequency-domain data. PAR reduction is achieved by multiplying independent phase sequences to the original data and determining the PAR of each phase sequence/data combination. The combination with the lowest PAR is transmitted. In other words, the data sequence $\boldsymbol{X}$ is element-wise phased by D N-length phase sequences, $\{\phi[k]^{(d)}\}_{k=0}^{N-1} = \boldsymbol{\phi}^{(d)}$, where d is an integer such that $d \in [0, D-1]$. After phasing, the D

candidate frequency-domain sequences are given by

$$\boldsymbol{X}^{(d)} = \boldsymbol{X} \circ e^{j\boldsymbol{\phi}^{(d)}}, \tag{36}$$

where $\circ$ is element-wise multiplication. We assume that $\boldsymbol{\phi}^{(0)} = 0 \; \forall \; k$ so that $\boldsymbol{X}^{(0)} = \boldsymbol{X}$.

Define the D candidate time-domain OFDM symbols $\boldsymbol{x}_L^{(d)} = IDFT_L\{\boldsymbol{X}^{(d)}\}$. Note that all of the candidate symbols carry the same information. In order to achieve a PAR reduction, the symbol with the lowest PAR is transmitted. We define

$$\tilde{d} = \underset{0 \leq d < D}{\arg\min} \; PAR\{\boldsymbol{x}_L^{(d)}\}. \tag{37}$$

Here, there is a choice of what oversampling factor should be used when selecting the minimum PAR signal. Ideally, L would be chosen large. However, as L grows so does the computational complexity of SLM. On the other hand, if L is too small, then peaks may regrow after oversampling. That is, $\tilde{d}$ may not be the same for every L.

3.1.1 Recovery of $\boldsymbol{X}$ in SLM

With $\tilde{d}$, the transmitted signal is $\boldsymbol{x}^{(\tilde{d})}$. In the receiver, $\boldsymbol{X}$ can be recovered with

$$\boldsymbol{X} = DFT\{\boldsymbol{x}^{(\tilde{d})}\} \circ e^{-j\boldsymbol{\phi}^{(\tilde{d})}} \tag{38}$$

$$= \boldsymbol{X} \circ e^{j\boldsymbol{\phi}^{(\tilde{d})}} \circ e^{-j\boldsymbol{\phi}^{(\tilde{d})}} \tag{39}$$

$$= \boldsymbol{X}. \tag{40}$$

To recover $\boldsymbol{X}$, it is necessary for the receiver to have a table of all $\boldsymbol{\phi}^{(d)}$ and some way of determining $\tilde{d}$. Determining $\tilde{d}$ can be done with $\lceil \log_2 D \rceil$ bits of side information or, as we advocate in Chapter 6, blindly without any side information.

One clever solution to the side information problem was presented in [29], where it was proposed that subcarrier interleaving be used to create different candidate signals in SLM (instead of phase rotations). In that case, several subcarriers need to be reserved for side information. With knowledge of which subcarriers have the side information, the receiver can recover it and de-interleave the data. The problem is that interleaving does not create sufficiently independent candidate signals. Accordingly, the PAR reduction performance of this technique suffers.

3.1.2 PAR Reduction

Ideally, a SLM scheme will create D *independent* mappings of a discrete-time domain signal $\boldsymbol{x}_L$. If we assume that each mapping is independent of all other mappings, then the CCDF of the PAR in a SLM scheme is simply

$$\Pr\left[PAR\{\boldsymbol{x}_L^{(\tilde{d})}\} > \gamma\right] = \Pr\left[\bigcap_{d=0}^{D-1}(PAR\{\boldsymbol{x}_L^{(d)}\} > \gamma)\right] \tag{41}$$

$$= \Pr\left[PAR\{\boldsymbol{x}_L\} > \gamma\right]^D. \tag{42}$$

For the $L = 1$, (42) simplifies to

$$\Pr\left[PAR\{\boldsymbol{x}^{(\tilde{d})}\} > \gamma\right] = \left[1 - (1 - e^{-\gamma})^N\right]^D. \tag{43}$$

Figure 12 is a plot of the theoretical PAR CCDF curves for a critically sampled OFDM symbol where $N = 64$. From the plot, we can see that large PAR reductions are possible with SLM. Figure 13 is a plot that illustrates the affect over sampling has on SLM. In the plot, the PAR CCDF curves are plotted for the critically-sampled OFDM symbol and for the $L = 4$ OFDM symbol. Also plotted are the PAR CCDFs when SLM ($D = 5$) is used to reduce the PAR. We can see that the PAR reduction for both cases is about the same at all probability levels. Finally, the PAR CCDF for an OFDM symbol that had been selected based on the Nyquist-samples, but had been oversampled back to $L = 4$ after selection is plotted. In a more perfect world this curve would exactly correspond with the $D = 5, L = 4$ CCDF, meaning that nothing is lost by applying SLM to the $L = 1$ OFDM symbols. However, the plot confirms that a certain amount of peak regrowth can occur when the critically-sampled symbol is used for selection.

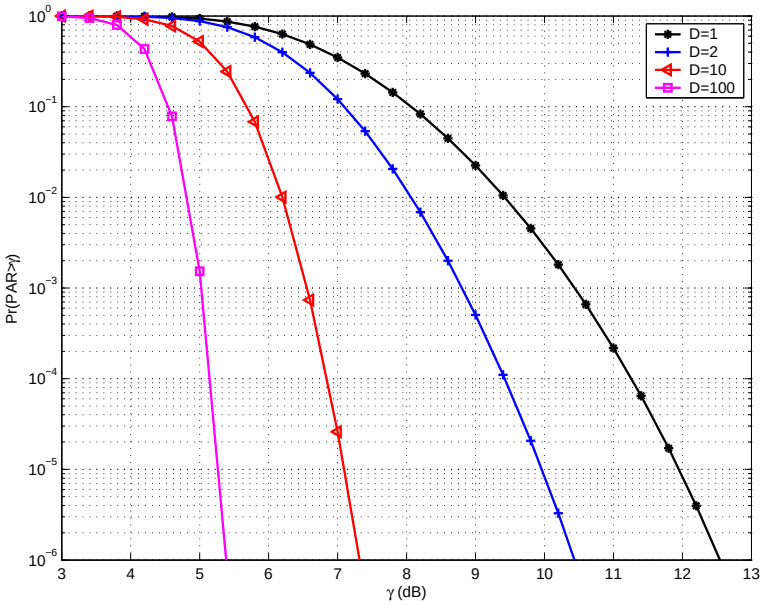

Figure 12: PAR CCDF of SLM for $N = 64$, $L = 1$ and $D = 1$, 2, 10, 100.

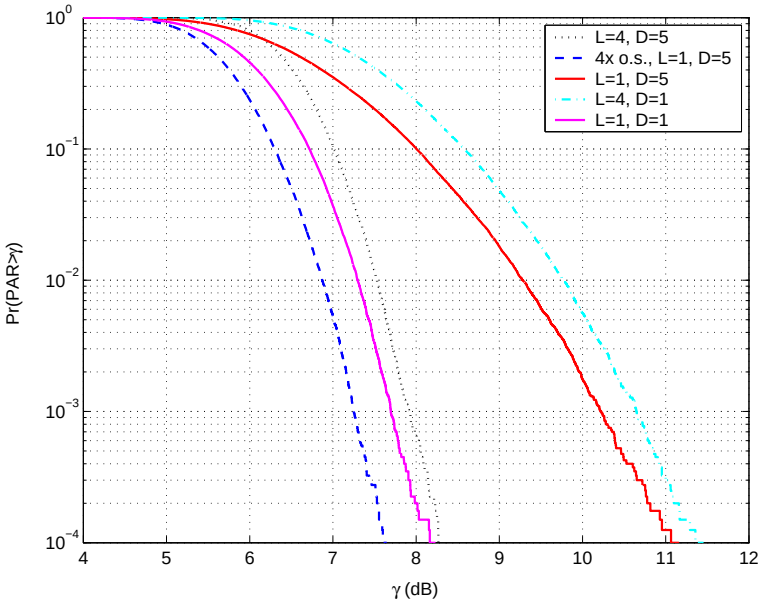

Figure 13: PAR CCDF of SLM for $N = 64$, $L = 1$, 4 and $D = 1$, 5. There is also a CCDF of the 4 times oversampled $D = 5, L = 1$ signals, which is a measure of the PAR regrowth from selecting on the critically sample values.

3.2 SLM Complexity

From Figure 12 it is obvious that SLM has significant PAR reduction capabilities. However, this reduction is not free. The most significant costs are the $D-1$ additional IDFT operations, and the $D-1$ N-length phase multiplications. These complexities can be mitigated slightly by using the inverse fast fourier transform (IFFT) in place of the IDFT and by using binary phase sequences so that all of the phase multiplications are just sign changes. Further complexity reductions can be made by implementing our proposed threshold SLM scheme that is described in Chapter 5.

In [39] a method was proposed that reduced the complexity of SLM. Recall that the IFFT algorithm works by using $R = \log_2 N$ stages of radix-2 decimation of the input sequence $\boldsymbol{X}$. Let us denote the output after the r^{th} stage by $IFFT^{(r)}\{\boldsymbol{X}\}$. The idea in [39] was to generate an intermediate IFFT of the data sequence, $IFFT^{(r_o)}\{\boldsymbol{X}\}$, and phase that sequence by phase vectors to create $IFFT^{(r_o)}\{\boldsymbol{X}\} \circ e^{j\boldsymbol{\phi}^{(d)}}$. This is a reduction in complexity because only $R - r_o$ IFFT stages need to be calculated in order to determine the PAR of each sequence. Mathematically, the candidate sequences in this scheme are

$$\boldsymbol{x}_L^{(d)} = IFFT_L^{(R-r_o)}\left[IFFT_L^{(r_o)}\{\boldsymbol{X}\} \circ e^{j\boldsymbol{\phi}^{(d)}}\right]. \tag{44}$$

There results show that for $N = 2^1 1$ they can use $r_o = 6$ without a noticeable reduction in PAR performance. This corresponds to a computational savings of 50%. This scheme is really just a reformulation of PTS with a random instead of structured search. But by putting in the context of SLM, the authors were able to make meaningful complexity-to-PAR tradeoffs.

3.3 Optimality Condition

SLM can be thought of as a method that randomly searches the "PAR space," where each phase mapping can be thought of as a one sampling from the PAR space. Intuitively, we would like to have independent "samples" in order to have the best chance of finding a low PAR. In [47] an attempt was made to find the determine the optimal type of phase sequences. By optimal, we mean the set of phase sequences that minimize the PAR CCDF. In that

paper, random, complementary Golay, Walsh-Hadamard, Shapiro-Rudin and orthogonal spreading variable factor (OVSF) sequences were all compared in the context of an SLM system. Through simulation, it was determined that the random sequences performed the best.

In [71], the problem of determining optimal phase sequences was also studied. From an intuitive perspective, it makes sense that in order to minimize the PAR, an SLM system should test independent mappings of $\boldsymbol{x}$. However, it was shown rigorously that $\boldsymbol{x}^{(m)}$ and $\boldsymbol{x}^{(l\neq m)}$ cannot be independent because they have $\boldsymbol{X}$ in common. More specifically, they showed rigorously that the forth order cumulant

$$cum\left[\boldsymbol{x}^{(m)}, (\boldsymbol{x}^{(m)})^*, \boldsymbol{x}^{(l\neq m)}, (\boldsymbol{x}^{(l\neq m)})^*\right] \neq 0, \tag{45}$$

which means that the mappings are mutually dependent.

However, if the following three conditions are met, then the second order cumulant, $\text{cum}\{\boldsymbol{x}^{(m)}, \boldsymbol{x}^{(l\neq m)}\} = 0$, which can be thought of as an approximate independence.

1. $E[e^{j\boldsymbol{\phi}^{(d)}}] = 0$.
2. $\boldsymbol{X}$ is i.i.d.
3. $\phi_k^{(d)}$ is i.i.d $\forall\ d > 0,\ k$.

There are many phase distributions that satisfy $E[e^{j\boldsymbol{\phi}^{(d)}}] = 0$ (i.e. uniform on $[0, 2\pi)$ or uniform discrete on $\{0, \pi\}$). Furthermore, it was also shown in [71] that if these conditions are not met, then the PAR CCDF will not be minimized. Figure 14 is an illustration of how $E[e^{j\boldsymbol{\phi}^{(d)}}] \neq 0$ is detrimental to PAR reduction. The simulation parameters for the plot are $N = 64$ and $D = 5$ for the lower two curves. From the plot, it is obvious that when $E[e^{j\boldsymbol{\phi}^{(d)}}] = 0$, the PAR CCDF is much better than when $E[e^{j\boldsymbol{\phi}^{(d)}}] = \pi/2 - 1 + j \neq 0$.

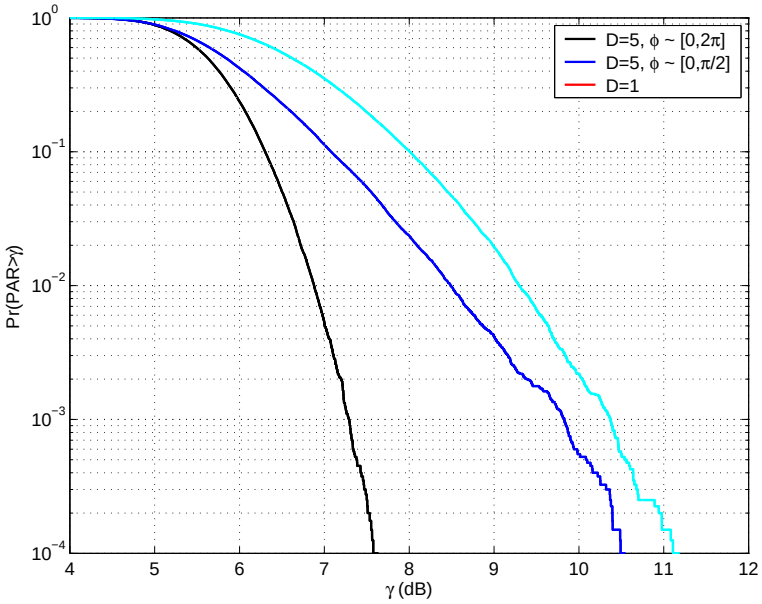

Figure 14: PAR CCDF of SLM for $N = 64$, $L = 1$ and $D = 1, 5$. For upper $D = 5$ curve $\phi_k^{(d)} \sim [0, \pi/2]$ so $E[e^{j\phi^{(d)}}] = \pi/2 - 1 + j \neq 0$. For the lower curve $\phi_k^{(d)} \sim [0, 2\pi]$ so $E[e^{j\phi^{(d)}}] = 0$.

3.4 Expected PAR Reduction

One measure of interest that we presented in [8] is the expected PAR in SLM. The result is surprisingly simple. From (43), we can determine that the CDF of the PAR of a discrete-time SLM signal is

$$F_{PAR}(x) = 1 - \left[1 - (1 - e^{-x})^N\right]^D. \tag{46}$$

The probability density function (PDF) is simply the derivative of the CDF,

$$f_{PAR}(x) = \Big[- D(1 - (1 - e^{-x})^N)^{D-1} \Big] \Big[- N(1 - e^{-x})^{N-1} \Big] e^{-x}. \tag{47}$$

Since $PAR \geq 1$, the expected value of the PAR is given by

$$E[PAR] = \int_1^\infty x \cdot f_{PAR}(x) dx. \tag{48}$$

In the appendix, we show that

$$E[PAR] = \frac{(D-1)!}{N} \sum_{k=1}^{N} \prod_{p=0}^{D-1} \frac{1}{(\frac{k}{N} + p)}. \tag{49}$$

Equation (49) shows that there is a simple closed form expression for the expectation of the PAR of a SLM signal for any N and D. The $D = 1$ case corresponds to expectation

Table 2: The PAR value corresponding to various Ds for different Ns.

	E[PAR] (dB)			
N	D = 1 (no SLM)	D = 2	D = 10	D = 30
64	6.76	6.08	5.04	4.55
128	7.35	6.76	5.88	5.48
256	7.87	7.35	6.59	6.25
512	8.34	7.87	7.20	6.91
1024	8.76	8.34	7.74	7.48

of the PAR of a discrete-time OFDM signal without SLM and simplifies to

$$E[PAR]\Big|_{D=1} = \sum_{k=1}^{N} \frac{1}{k}, \tag{50}$$

which is the N^{th} harmonic number.

This is an interesting result when taken in light of the commonly-cited worst-case PAR for a given N, which assumes all of the subcarriers are the same symbol. In that case $PAR = N$. Equation 50 reveals that the E[PAR] increases much slower than linearly; in fact, even for $N = 2^{27}$, E[PAR] is only 12.8 dB. Table 1 gives several examples of E[PAR].

Figure 15 is a plot of the sample average PAR ($\hat{\mu}$) versus the theoretical E[PAR] for OFDM signals where the frequency domain symbols were taken from the 16PSK or 16QAM constellations. It shows that the theoretical E[PAR] is very close to the sample estimates even for small N. This result is important as a way of verifying that the errors associated with the commonly made assumptions are very small. Figure 16 is a plot theoretical trend of the expected PAR versus N for $D = 1, 2, 4, 32$.

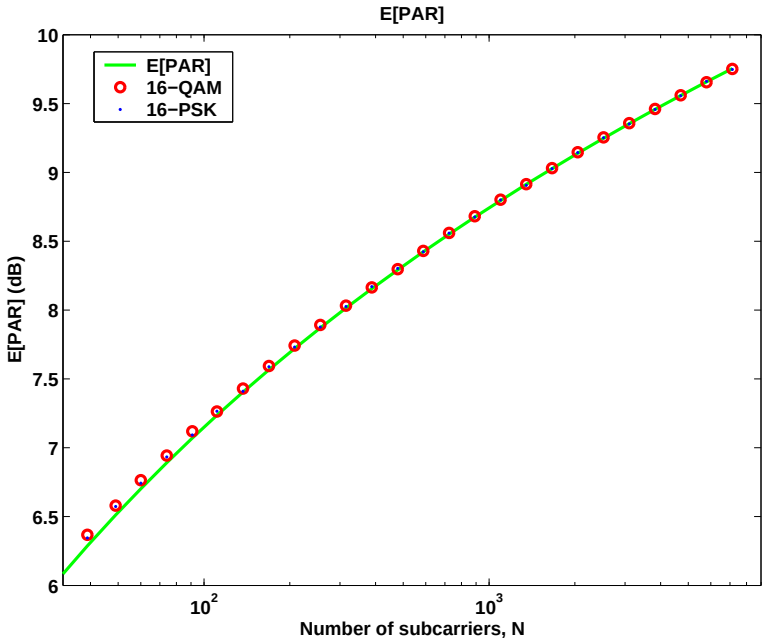

Figure 15: The sample means versus the theoretical E[PAR] when X_k is taken from 16PSK or 16QAM. 30,000 OFDM blocks were used to obtain the sample mean estimates.

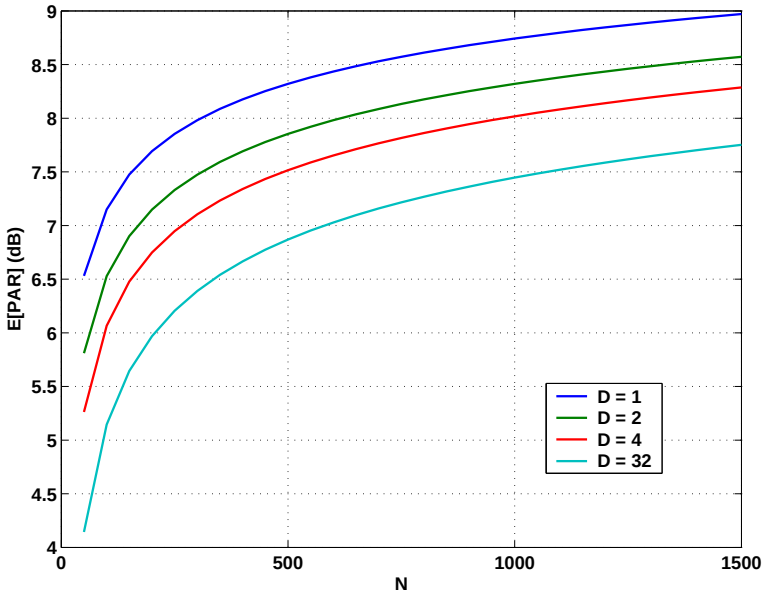

Figure 16: Theoretical trend of the expected PAR versus N for $D = 1, 2, 4, 32$.

3.5 Conclusions

In this chapter we have presented the selected mapping PAR reduction method. It was demonstrated that large PAR reduction are possible with SLM. The complexity of SLM was presented as well as an analysis of the loss of PAR reduction performance due to selection with the critically sample OFDM symbol. Additionally, a summary of the SLM optimality conditions from [71] was given. Finally, the expected PAR value in SLM was derived and analyzed.

3.6 Derivation of E[PAR]

The expectation is given by

$$E[PAR] = \int_1^\infty x \; f_{PAR}(x)dx. \tag{51}$$

The integral above yields a messy result because the lower limit is one, which is due to the fact that $PAR \geq 1$. However, as $N \to \infty$ the lower limit on the expectation integral can be changed from one to zero. In practice, altering the limits of the integral, even for $N = 20$, only yields an error of 10^{-5}. And for practical values, where $N \geq 64$, the error is less than 10^{-11}. It is also important to note that the complex Gaussian assumption made in deriving the PDF in (47) is more likely to introduce error than the limit change. Thus, we have

$$E[PAR] \overset{N\to\infty}{=} \int_0^\infty x \; f_{PAR}(x)dx. \tag{52}$$

With a simple change of variables ($x \triangleq 1 - (1 - e^{-u})^N$) we have

$$E[PAR] = \int_1^0 Dx^{D-1} \ln\left[1 - (1-x)^{\frac{1}{N}}\right]dx. \tag{53}$$

Note that with

$$\int \ln[1 - (1-x)^{\frac{1}{N}}]dx = x[\ln(1 - (1-x)^{\frac{1}{N}})] + \sum_{k=1}^{N} \frac{1}{k}[(1-x)^{\frac{k}{N}} - 1] \tag{54}$$

the expectation integral becomes an integration by parts problem. Let's define two functions, R and G in order to use simpler expressions:

$$\begin{aligned} R(x,N) &\triangleq x[\ln(1 - (1-x)^{\frac{1}{N}})] + \sum_{k=1}^{N} \frac{1}{k}[(1-x)^{\frac{k}{N}} - 1] \\ G(x,N) &\triangleq \sum_{k=1}^{N} \frac{1}{k}[(1-x)^{\frac{k}{N}} - 1]. \end{aligned} \tag{55}$$

Now the indefinite expectation integral, (53), becomes

$$\begin{aligned}&\int x^{D-1}\ \ln[1-(1-x)^{\frac{1}{N}}]dx\\&= x^D\ R(x,N) - (D-1)\int x^{D-1}[\ln(1-(1-x)^{\frac{1}{N}})]dx - (D-1)\int x^{D-2}G(x,N)dx.\end{aligned} \tag{56}$$

If we move the middle term on the right hand side of (56) to the left hand side, we have

$$D\ \int x^{D-1}\ \ln[1-(1-x)^{\frac{1}{N}}]dx = x^D\ R(x,N) - (D-1)\int x^{D-2}G(x,N)dx. \tag{57}$$

The left over integral can also be done with integration by parts. The result is

$$\begin{aligned}&D\ \int x^{D-1}\ \ln[1-(1-x)^{\frac{1}{N}}]dx\\&= x^D\ R(x,N) - \sum_{q=1}^{D-1}\left\{(-1)^{q+1}x^{D-1-q}\cdot\sum_{k=1}^{N}\left[\frac{(-1)^q\ (1-x)^{\frac{k}{N}+l}}{k\ \prod_{p=1}^{q}(\frac{k}{N}+p)} - \frac{x^q}{k\ q!}\right]\prod_{l=1}^{q}(D-l)\right\},\end{aligned} \tag{58}$$

which we define as $\Upsilon(x,N,D)$. Therefore,

$$E[PAR] = \Upsilon(0,N,D) - \Upsilon(1,N,D). \tag{59}$$

After simplification, $\Upsilon(1,N,D)$ becomes

$$\Upsilon(1,N,D) = -\sum_{k=1}^{N}\frac{1}{k} - \sum_{q=1}^{D-1}\sum_{k=1}^{N}\frac{(-1)^q}{k\ q!}\prod_{l=1}^{q}(D-l). \tag{60}$$

It can be shown that $\frac{1}{q!}\prod_{l=1}^{q}(D-l) = \binom{D-1}{q}$. Thus, $\Upsilon(1,N,D)$ is the alternating sum of a binomial series which is $0\ \forall\ N$ and D:

$$\Upsilon(1,N,D) = \sum_{q=0}^{D-1}\sum_{k=1}^{N}\frac{(-1)^{q+1}}{k}\binom{D-1}{q} = 0. \tag{61}$$

Therefore the expectation of the PAR is $\Upsilon(0,N,D)$. Observe that all terms of (58) in the summation over q go to zero except $q = D-1$; thus,

$$E[PAR] = \frac{(D-1)!}{N}\sum_{k=1}^{N}\prod_{p=0}^{D-1}\frac{1}{(\frac{k}{N}+p)}. \tag{62}$$

CHAPTER IV

NET POWER SAVINGS IN SELECTED MAPPING

As was outlined in Chapter 1, there has been alot of attention devoted to reducing the PAR in OFDM. Accordingly, it is important to provide an analysis of the power savings that result from PAR reductions. A net power savings analysis must include all additional power resources that a PAR reduction scheme uses. This includes any additional computational complexity beyond the requirements of traditional OFDM. Additional complexity requires both time and, more importantly, power consumption in the processor. Therefore, it is also important to analyze the computational power costs of implementing a PAR reduction scheme in order to determine if the power costs from the processor outweigh the power saved by peak reduction[1].

4.1 Introduction

In a practical system, prior to transmission, the OFDM signals are sent through a PA which is always peak-power limited. If $|x(t)|^2$ is larger than the saturation point of the PA at any time t, then $x(t)$ will be clipped. Clipping is a type of signal distortion, which results in decoding errors at the receiver or, equivalently, an increased BER (see Section 2.2.1). PAR is critically important to practical ODFM system design because it can be used as a measure of the clipping probability. In our analysis we assume that the OFDM system must provide a fixed clipping probability, which approximately corresponds to a fixed BER.

In [45] it was demonstrated that the complementary cumulative distribution function (CCDF) of the PAR of a continuous-time OFDM signal $x(t)$ can be expressed as

$$\Pr(PAR > \gamma) = 1 - \exp\left[- \sqrt{\frac{\pi\gamma}{3}} N e^{-\gamma} \right], \tag{63}$$

which agrees with simulations for $N \geq 64$. From (63) we can find the PAR as a function of

[1]This chapter was published in [10] and is a result of a collaboration with G. Tong Zhou

Table 3: The PAR value corresponding to various probability-of-clipping levels for different Ns.

	PAR (dB)				
N	64	128	256	512	1024
$p = 10^{-2}$	9.97	10.3	10.6	10.8	11.1
$p = 10^{-3}$	10.9	11.2	11.4	11.6	11.8
$p = 10^{-4}$	11.7	11.9	12.1	12.3	12.5
$p = 10^{-5}$	12.3	12.5	12.7	12.8	13.0
$p = 10^{-6}$	12.9	13.1	13.2	13.4	13.5

the probability level, p.

$$PAR(p) = \frac{-1}{2} W\bigg(-6\frac{\ln(1-p)^2}{\pi N^2}\bigg), \tag{64}$$

where W is Lambert's W-function given by the inverse of $f(W) = We^W$ [67]. Table 3 summarizes several PAR values for various p.

As we can see from Table 4.1, PAR(p) has a strong dependence on the probability of clipping. Therefore, we must choose a probability of clipping that is reasonable in practical applications in order to obtain meaningful power savings results. In [60] there is a thorough treatment of how clipping leads to increased BER and spectral regrowth. Obviously we would like to minimize the BER, but in a practical system the spectral regrowth must also be kept to a minimum to prevent adjacent channel interference.

It is important to note that the probability-of-clipping levels are given as the probability that any part of an OFDM symbol is clipped, where each OFDM symbol contains N data symbols. It may be intuitive to think there is a trivial relationship between the probability of clipping and the BER; however, the relationship is quite complicated. This is because the receiver performs a FT operation on the clipped frame and the effects of the clipping propagate to all data symbols in the frame. In [60], Tellado explored the SER/clipping relationship and found that the BER is actually a strong function of the size of the symbol constellation. That is, for the same probability of clipping, a constellation with 4QAM would incur fewer symbol errors than 256QAM.

Because BER constraints vary according to application and there are many variables involved in relating a probability-of-clipping level to a BER, in this paper we will assume

that a probability-of-clipping level of 10^{-4} is reasonable.

4.2 Power Amplifier Efficiency

For simplicity, let us consider Class A PAs which are the most linear. They consume a constant amount of power, P_{DC}, regardless of the input power. The PA efficiency, η, is defined as the portion of P_{DC} that is delivered to the load; i.e., $\eta = P_{out,ave}/P_{DC}$ [22]. For a given OFDM signal, we need to adjust the average input power so that the peaks of the signal are rarely clipped. That is, we will have to apply an input backoff (IBO) to the signal prior to amplification. The amount of the IBO directly relates to both the PAR and η: large PARs lead to increased IBO and reduced η. With the probability of clipping analysis from the previous section we can define the IBO as equal to the PAR for a certain probability of clipping. Class A PAs have a maximum η of 50% [22]. We shall assume an ideal linear model [22] for the PA, meaning that linear amplification is achieved up to the saturation point. Under these conditions,

$$\eta = \frac{0.5}{PAR}. \tag{65}$$

For an OFDM signal with 128 subcarriers, in order to guarantee that no more than 1 in 10,000 frames are clipped, we have to apply an IBO that is equivalent to the PAR at the 10^{-4} probability level. From Table 2, the corresponding $PAR = 11.9dB$ (15.5). Thus, to amplify a 128-carrier OFDM signal with a Class A PA under the constraint that the clipping probability should not exceed 10^{-4}, the PA efficiency becomes $\eta = 0.5/PAR = 0.5/15.5 = 3.2\%$. Such a low power efficiency is a strong motivation for us to pursue PAR reduction. With a Class A PA, every 3dB of PAR reduction translates into doubling of the PA efficiency.

For the following power savings analysis we will assume that a fixed $P_{out,ave}$ is required for the system and that the transmission PA can be re-biased according to any PAR change. So for any PAR reduction, the PA will produce the same $P_{out,ave}$ as before the reduction, but the P_{DC} will be lowered, leaving a power savings. Figure 17 is a graphical illustration of this concept, assuming an ideal linear PA. Consider the solid line to be the PA transfer

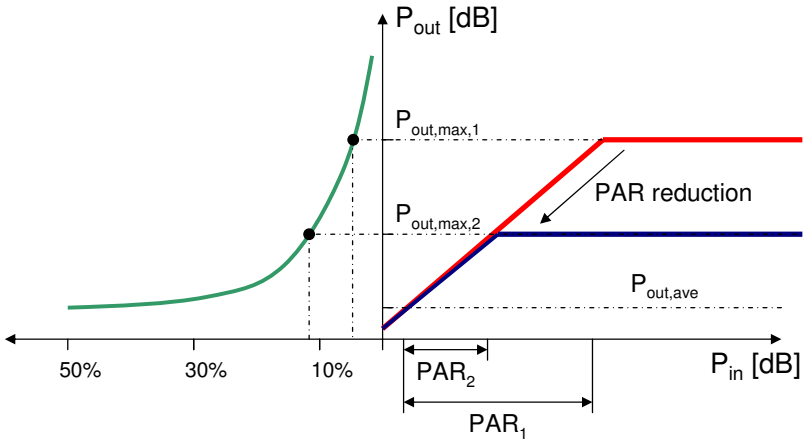

Figure 17: PA response before and after PAR reduction. The left plot shows how the power efficiency varies with PAR.

characteristic prior to PAR reduction. In this case $P_{out,ave} = 1W$, $P_{out,max,1} = P_{sat} = 12W$ and, for a Class A PA, $P_{DC} = 2P_{sat} = 24W$. If $P_{out,ave}$ is held constant, and the PAR is reduced from 12 to 6, then $P_{out,max,2} = P_{sat} = 6W$ and $P_{DC} = 2P_{sat} = 12W$. Therefore, a PAR reduction from 12 (10.8dB) to 6 (7.8dB) (-3dB change) resulted in a $12W$ power savings.

We can quantify the power savings by first relating the power consumption P_{DC} to η:

$$P_{DC} = \frac{P_{out,ave}}{\eta}. \tag{66}$$

Substituting (65) into (66), we infer that any power saving from one efficiency to another, $\eta_1 \rightarrow \eta_2$, can be expressed by

$$\begin{aligned} P_{savings} &= P_{DC,1} - P_{DC,2} \\ &= 2P_{out,ave}(PAR_1 - PAR_2), \end{aligned} \tag{67}$$

Several promising methods currently being developed that increase PA η without PAR reduction include adaptive biasing, linear amplification using non-linear components (LINC), feedforward or predistortion linearization, and the Doherty amplifier [22]. However, all of these methods involve hardware implementations that can be expensive. Alternatively, power savings can be achieved with PAR reduction methods that are implemented in software. To calculate the power savings as the result of a PAR reduction algorithm, we simply substitute $P_{out,ave}$ and the PAR difference (in linear scale) into (67).

4.3 Power Savings Through Selected Mapping

As outlined in Chapter 3, SLM has emerged as a promising way to reduce the PAR of OFDM signals. SLM takes advantage of the fact that the PAR of an OFDM signal is very sensitive to phase shifts in the frequency-domain data. PAR reduction is achieved by multiplying independent phase sequences with the original data and determining the PAR of each phase sequence/data combination. The combination with the lowest PAR is transmitted. In [69] it was demonstrated that the side information in SLM does not need to be transmitted, but, can instead be blindly detected at the receiver with negligible increase in BER . The only cost of SLM is in additional processing. Because the PAR of each of D phase sequence/data combinations must be found, D additional IFFTs are needed at the transmitter, which translates to increased processor power consumption. Furthermore, D phase sequences must be stored or generated on demand, and either option will incur additional power consumption. This section will concentrate on power savings that result for SLM's PAR reduction capabilities.

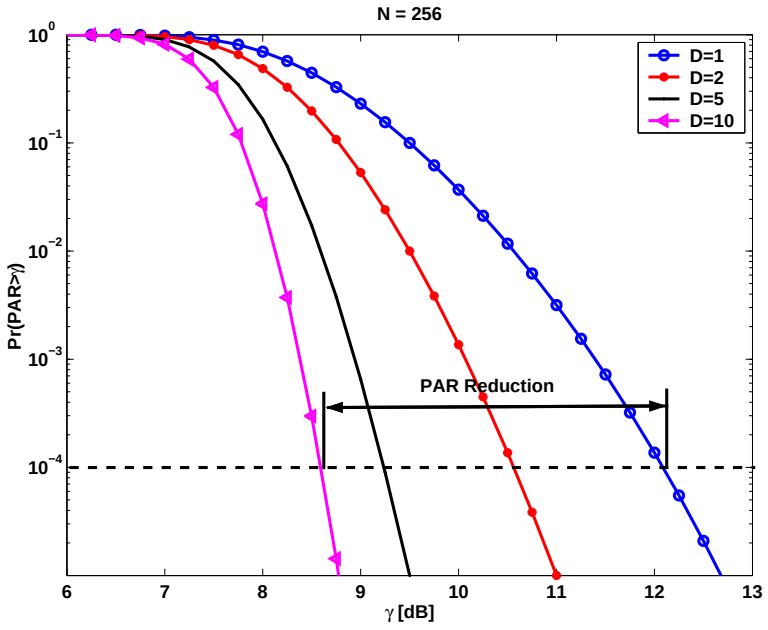

Figure 18: CCDF for SLM where $N = 256$ and $D = 1, 2, 5, 10$.

The CCDF of a SLM signal is simple if we assume that each of the D time-domain signals tested are independent of the other generated signals. This assumption is not strictly valid

Table 4: For $N = 256$, the PAR value (in dB and linear scales) corresponding to the 10^{-4} probability-of-clipping level for different Ds. The savings gain, G_s, equals twice the PAR reduction amount (in linear scale)

D	PAR (dB)	PAR	G_s
1 (no SLM)	12.1	16.2	0
2	10.6	11.5	9.5
3	9.9	9.8	12.8
4	9.5	8.9	14.5
5	9.2	8.3	15.6
10	8.6	7.2	17.9

because all D of the generated signals have the original frequency-domain data in common. Nevertheless, the resulting approximation is very close to simulation results. With the independence assumption, the probability of clipping becomes

$$\Pr(PAR > \gamma) = \left[1 - \exp\left(- \sqrt{\frac{\pi\gamma}{3}} N e^{-\gamma} \right) \right]^D. \tag{68}$$

From Figure 18 it is obvious that SLM can achieve substantial PAR reductions. The inverse of (68) is the PAR for a given probability level, p,

$$PAR(p) = \frac{-1}{2} W\left(- 6 \frac{\ln(1 - \exp[\frac{\ln(p)}{D}])^2}{\pi N^2} \right), \tag{69}$$

where W is Lambert's W-function given by the inverse of $f(W) = We^W$ [**?**]. Let us define the savings gain, G_s as the ratio of power saved to the average output power, i.e., $G_s = P_{save}/P_{out,ave}$. From 67, we infer that

$$G_s = 2(PAR_1 - PAR_2). \tag{70}$$

Table 4 gives several PAR and G_s values of the SLM case over the no SLM ($D = 1$) case assuming $N = 256$ and $p = 10^{-4}$. It is evident from Table **??** that SLM can achieve significant PAR reductions and power savings, even for small D.

In order to determine practical power savings, it is important to examine an appropriate range of $P_{out,ave}$. To gain some perspective, consider that the Federal Communications Commission (FCC),which is the regulatory body for wireless communications in the United States, specifies that the effective isotropic radiated power (EIRP) be no more than 4 watts

in the unlicensed ISM and UNII bands [1]. Since this Figure is the EIRP, it includes antenna gain, G_a, which can be assumed to be between 2dB (1.6) and 8 dB (6.3) for portable devices [54]. The PAR also comes into consideration because 4 watts is the *maximum* EIRP, so $P_{out,ave}$ is a factor of PAR lower than $P_{out,max} = P_{out,ave}PAR$. Therefore, assuming a representative PAR of 10dB, according to

$$P_{out,ave} = \frac{4W}{G_a PAR}, \tag{71}$$

it is appropriate to assume that the transmitting PA must produce $63mW \leq P_{out,ave} \leq 250mW$. SLM becomes more attractive as $P_{out,ave}$ becomes larger.

Through evaluation we have found that $P_{savings}$ in equation (67) is independent of the value of N for $N < 2^{25}$. This means that the difference between two PARs from (69) with different Ns is constant for $N < 2^{25}$. Figure 19 is a plot of the power saved through SLM for a Class A PA. Note that the power savings is on the order of several Watts for

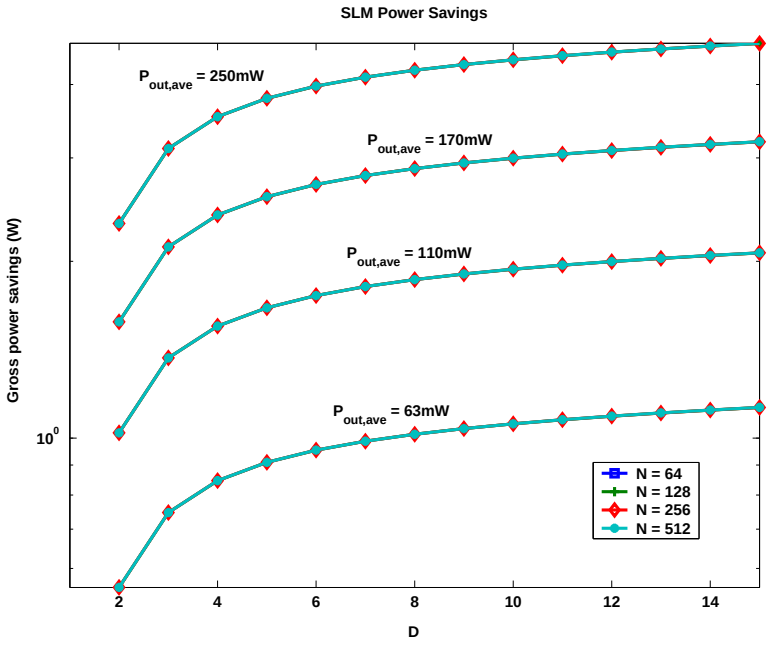

Figure 19: Power saving of SLM at different Ns and Ds and $P_{out,ave}$s.

$P_{out,ave} > 110mW$.

Table 5: Relevant data for the TI C55x DSP [3].

Current/Processor cycle/Second	0.33 mA/MHz
Supply voltage	12.6 V
Processor frequency	200 MHz
Cycles/256-point FFT	4786
Cycles/Radix 2 FFT core	5
Overhead cycles/FFT	306
Cycles/N-point FFT	$306 + 5\frac{N}{2}\log_2(\frac{N}{2})$
Cycles/D-length minimum-index search	$17 + D/2$
Cycles/N-length maximum-value search	$N/2 + 6$
Multiplies/Cycle	2
Additions/Cycle	4
Cycles/Complex Multiply	3

4.4 Power Costs of Selected Mapping

As was mentioned in the last section, SLM does consume additional processing power. It is only reasonable to consider whether the processer power consumption outweighs the power savings from PAR reduction. For this purpose we will consider Texas Instrument's C55x series DSPs in all computation comparisons. Table 5 summarizes the relevant data for the TI C55x DSP which can be found in [3]. Table 6 summarizes the processing power required for FFTs of different lengths.

The energy consumption per cycle is

$$Energy/cycle = 0.33\frac{mA \cdot sec}{Mcycle}1.26V = 415.8\frac{pWsec}{cycle}. \tag{72}$$

Thus, the energy consumption per length of FFT/IFFT, assuming the length is a power of two, is

$$\begin{aligned} Energy/point &= 415.8\tfrac{pWs}{cycle}\left[306 + 5\tfrac{N}{2}\log_2(\tfrac{N}{2})\right]cycle \\ &= \left[127.2 + 1.04N\log_2(\tfrac{N}{2})\right]nJ. \end{aligned} \tag{73}$$

For comparison purposes it is assumed that the PA and the DSP work for the same amount of time. This way they can be compared in terms of power consumption instead of energy consumption.

Table 6: Power consumption for different FFT lengths, N.

N	Power (μW)
32	0.260
64	0.459
128	0.926
256	1.99
512	4.39

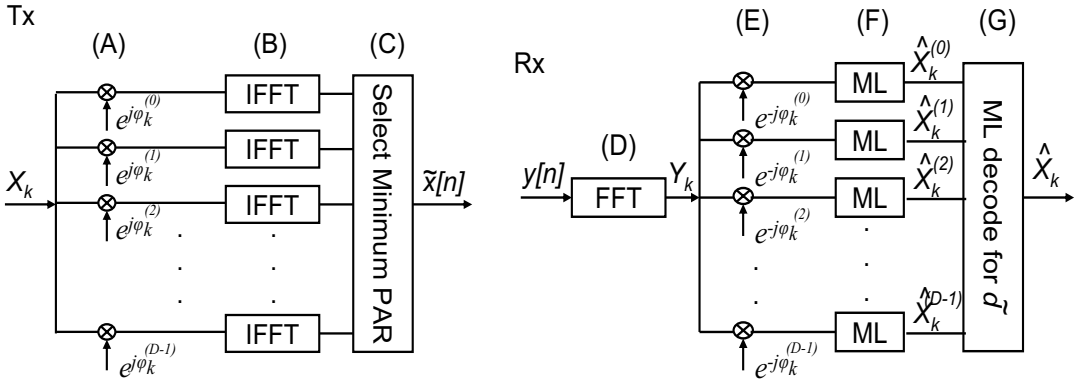

(a) Transmitter (b) Receiver

Figure 20: Blind SLM OFDM block diagram. Each part of the system that requires processor resources is labelled with a letter, (A) through (G).

As can been seen in Figure 20, the Nyquist-sampled Blind SLM (BSLM) transmitted signal is $\tilde{x}[n]$, which is defined according to

$$\begin{aligned} \tilde{d} &= \arg\min_{0\le d\le D-1} PAR\{IDFT(X_k\ e^{j\phi_k^{(d)}})\}, \\ \tilde{x}[n] &= IDFT(X_k\ e^{j\phi_k^{(\tilde{d})}}), \end{aligned} \tag{74}$$

where D is the number of phase mappings tested, $\{\phi_k^{(d)}\}_{d=0}^{D-1}$ are the phase sequences (it is assumed that $\phi_k^{(0)} = 0, \forall\ k$) , $\{X_k\}_{k=0}^{N-1}$ is the frequency domain data, and N is number of subcarriers. Then, according to Figure 20, at the transmitter, BSLM incurs additional processing requirements at points (A), (B), and (C).

In order to analyze the computational requirements for BSLM we will examine the implementation presented in [69]. In [69] it was shown that with $\phi_k^{(d)} = a_d\ k^3$, where a_d is a constant, excellent PAR reduction performance can be achieved with the benefit of a simplistic formula for generating $\phi_k^{(d)}$.

In Figure 20, (A) corresponds to the phase sequence creation and multiplication. For this analysis we will consider that the each phase sequence is generated on demand; thus $3N$ multiplies are necessary for each sequence ($a_d\ k \cdot k^2$). Also, because the data is complex, $(D-1) \cdot N$ complex multiplies are necessary at (A). It could be assumed that the phase sequences, $\{\{e^{ja_d k^3}\}_{k=0}^{N-1}\}_{d=0}^{D-1}$, are stored in a look-up table instead of being generated on demand. However, it is very difficult to quantify the memory power usage that results from storing the sequences. (B) corresponds to the D IFFTs that are necessary in order to find the PAR of each mapping, which is $D-1$ more than are necessary in traditional OFDM operation. Finally, (C) corresponds to the process of selecting the mapping with minimum PAR. This involves a N-length maximum value search to find the PAR of each mapping and a D-length minimum index search to determine and select the mapping with the lowest PAR.

At the receiver, the first block, (D), is a FFT which is necessary in any OFDM system. At (E), the receiver must multiply $D-1$ inverse phase sequences by $\{Y_k\}_{k=0}^{N-1}$. As in the transmitter, the receiver is assumed to have created the phase sequences on demand with $3N$ multiplies. At (F), the receiver must perform a minimum-distance maximum-likelihood (ML) decoding to determine which of the constellation points, $\{C_m\}_{m=0}^{Q-1}$, that each point, k, of each mappings, d, of $\{\{Y_k^d\}_{k=0}^{N-1}\}_{d=0}^{D-1}$ corresponds to. To find the square distance, $\mathcal{D}$, between any two points requires 3 additions and 2 multiplies. Therefore, (F) requires a total of $3N \cdot Q$ additions, $2N \cdot Q$ multiplies and N Q-length minimum-index searches for each mapping. In BSLM it is also necessary to identify which phase sequence was used in transmission. This is done at (G). Since $\{a_d\}_{d=0}^{D-1}$ is taken from a known set, we can define the set of square distances, $\{\mathcal{D}_k^{(a_d)}\}_{k=0}^{N-1}$, between Y_k and the optimal constellation points as found in (F) for each possible a_d. Thus, the transmitted sequence corresponds to the a_d that minimizes

$$g(a_d) = \sum_{k=0}^{N-1} \mathcal{D}_k^{(a_d)} \tag{75}$$

over $0 \leq d \leq D-1$. Therefore, (G) requires $N \cdot D$ additions and a D-length minimum-index search.

Table 7 summarizes the additional operations necessary for BSLM.

Table 7: Additional operations necessary in BSLM for constellation size Q, data length N, and D cubic phase sequences.

Operation	Transmitter	Reciever
IFFT	$D-1$	0
Multiplies	$3N(D-1)$	$2NQ(D-1)$ $+3N(D-1)$
Complex Multiplies	$N(D-1)$	$N(D-1)$
Additions	0	$3NQ(D-1)$ $+ND$
D-length min-index search	0	1
Q-length min-index search	0	$N(D-1)$
N-length max-value search	0	D

Figure 21 is a plot of the power consumed by BSLM for various D, N with $Q = 16$. Note that the power consumption is on the order of tens of μW, whereas the savings was on the order of Watts. Obviously BSLM is capable of producing a large net power savings. This savings is quantified in Figure 22, which is based on a probability of clipping of 10^{-4}. From the plot we can see that by employing only one additional phase mapping, $D = 2$, a 1 W power savings can be achieved for $P_{out,ave} = 110$ mW. Note that from Table 2 and eq. (6) we see that the $P_{DC} = 2P_{out,ave}16.2 = 3.6$ W before PAR reduction for $P_{out,ave} = 110$ mW, so a 1W savings ($D = 2$) corresponds to a reduction in the DC power by 28%. It is also important to notice that the power savings curves level off for large D, which is a result of the diminishing PAR reduction capability of SLM as D grows. Finally, we can see that the minuscule power cost of SLM is far less than the power saved.

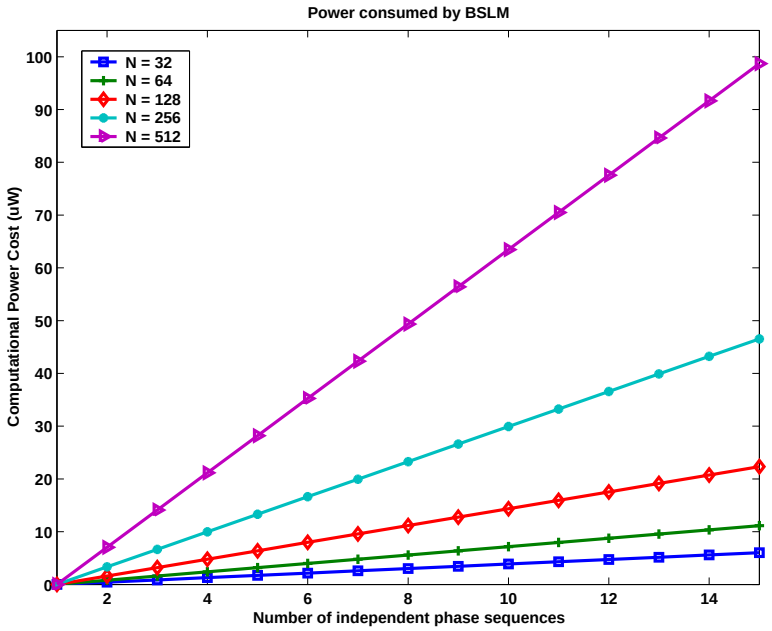

Figure 21: Power consumed by BSLM for various D, N with $Q = 16$.

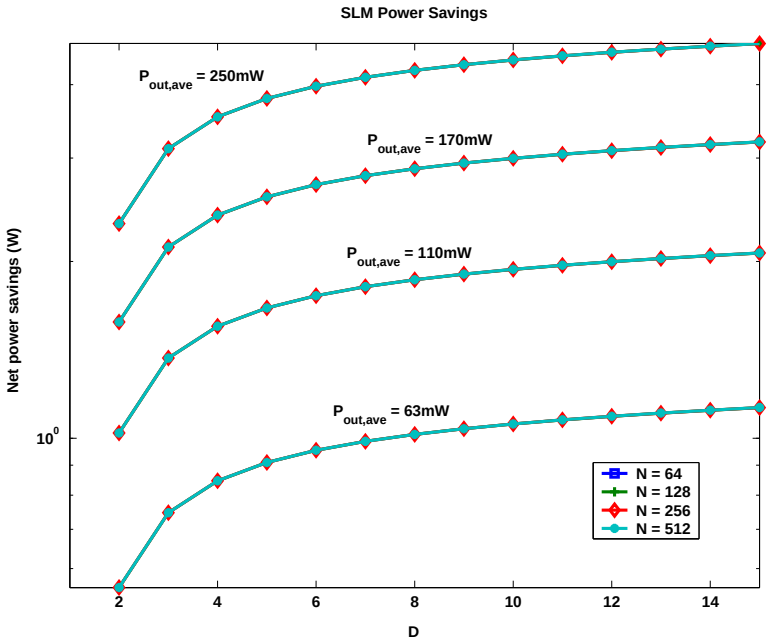

Figure 22: Net power saving of blind-detection SLM at different Ns and Ds and $P_{out,ave}$s for a probability of clipping of 10^{-4}.

4.5 Conclusions

In this chapter we have detailed our analysis of the net power savings when SLM is used to reduce the PAR of OFDM signals. It has been well established that PAR reduction leads to power savings, and we were able to quantify this savings in terms of real-world devices. We also accounted for the computational power consumption that occurs in the implementation of SLM.

We found that the net power savings is directly proportional to the desired average output power, $P_{out,ave}$, and is highly dependent on the clipping probability level. Accordingly, we determined realistic values for each parameter. $P_{out,ave}$ is on the order of $100mW$, while 10^{-4} is an acceptable clipping probability. With these parameters the net power savings is quite significant and is on the order of several Watts.

CHAPTER V

THRESHOLD SELECTED MAPPING

The idea of thresholding the PAR of a SLM system was first mentioned in [29]. However, that work dealt with an interleaving SLM method and thresholding the PAR was only mentioned in passing without any analysis. Threshold PAR was as it is presented here was originally developed in [8] in the context of reducing the computational complexity of SLM. In [12] it was noted that thresholding the PAR in SLM can lead to better blind detection rates, which was rigorously studied in [9].

5.1 Preliminaries

Let us consider a practical transmission system and the role that PAR reduction plays in it. We consider the case where the power amplifier (PA) is not adaptively biased, which means that the system is designed with a certain constant clipping threshold. For example, class A amplifiers require a bias power that is twice the clipping threshold [22].

The goal of PAR reduction is to increase power efficiency while keeping the probability of clipping at an acceptably low level. Clipping needs to be minimized because it is a distorting operation that increases the error rate. Accordingly, let us quantify clipping in a transmission system by two parameters: the (power) clipping level, γ_o, and the probability of clipping, Pr(PAR$>\gamma_o$) (assume the average power is normalized to one). For instance, a system with $\gamma_o = 7$dB that is able to tolerate at most 1 clipped OFDM symbol in 10,000 would have Pr(PAR$>\gamma_o$) $\triangleq p = 10^{-4}$.

Because the PA is not adaptively biased the power efficiency of the system is determined exclusively by the average symbol power ($E[|x[n]|^2]$) and the bias point of the PA, neither of which is changed dynamically. The point is, that once the system is designed for a certain PAR, any further PAR reduction is pointless.

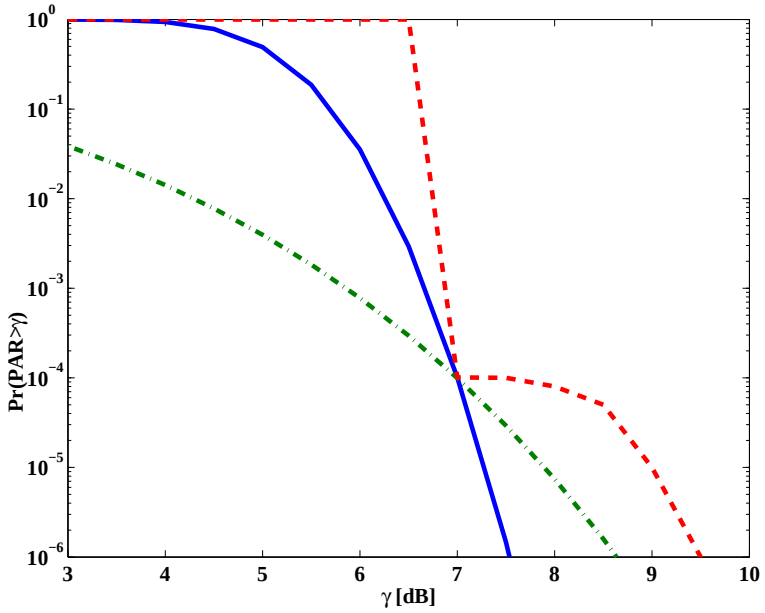

Figure 23: Different CCDFs that all pass through the point (7dB, 10^{-4}). We show that in a practical system designed for a probability of clipping of 10^{-4} and clipping level of 7dB, these curves all have the same power efficiency performance.

Figure 23 is an illustration of this concept through the complementary cumulative distribution function (CCDF) curves. Notice that all of the curves pass through the point (7dB, 10^{-4}), but they all correspond to different distributions. For a system designed around these parameters (γ_o = 7dB, $p = 10^{-4}$), each of the curves has the same power efficiency and clipping probability. Therefore, if some modification that increases the blind detection rate also changes the shape of the CCDF from one curve to another in Figure 23, the system will not be sacrificing any PAR reduction performance.

The consequence of all of this analysis is that a SLM system only has to test phase sequences until a signal with a PAR$< \gamma_o$ is found. It is possible that further phase mappings could produce an even lower PAR signal, but we just established that any further PAR reduction will not further improve the power efficiency for a given PA with a fixed bias and probability of clipping. It is also possible that after $D_{\max}$ mappings the PAR is still larger than the clipping level. In this case the signal is simply sent despite the fact that it will be clipped in the PA. Note, however, that $D_{\max}$ is chosen to ensure that the probability of clipping is kept to the specified level.

It has been shown in Chapter 3 that the CCDF of the PAR in a Nyquist sampled OFDM symbol is

$$\Pr(PAR_{SLM} > \gamma) = \left[1 - (1 - e^{-\gamma})^N\right]^D, \tag{76}$$

where N is the number of subcarriers and D is the number of independent phase mappings. For future brevity we will define

$$\Gamma^N \triangleq (1 - e^{-\gamma})^N \tag{77}$$

$$\Gamma_o^N \triangleq (1 - e^{-\gamma_o})^N. \tag{78}$$

If the SLM process stops when PAR$< \gamma_o$ then we can solve for $D_{\max}$ to guarantee that Pr(PAR$> \gamma_o) \leq p$.

$$p \geq \left(1 - \Gamma_o^N\right)^{D_{\max}} \tag{79}$$

$$\Rightarrow \quad D_{\max} = \left\lceil \frac{\ln(p)}{\ln(1 - \Gamma_o^N)} \right\rceil, \tag{80}$$

where $\lceil a \rceil$ is the "ceil" operation that returns the smallest integer greater than or equal to a.

In some systems it may be more appropriate to design a system around the number of mappings $D_{\max}$. This is the case when the application cannot tolerate additional computational time that extra mappings would contribute. If we choose the probability of clipping p to be the dependent variable, we have

$$p = \left(1 - \Gamma_o^N\right)^{D_{\max}}, \tag{81}$$

and if γ_o is the dependent variable, then

$$\gamma_o = -\ln\left[1 - (1 - e^{\ln(p)/D_{\max}})^{1/N}\right]. \tag{82}$$

In other words, there are three system parameters, $(p, \gamma_o, D_{\max})$, any two of which determine the third. Figures 24 and 25 illustrate this concept. Figure 24 shows several CCDFs where γ_o and p are specified and determine the value of $D_{\max}$. Figure 25 shows several CCDFs where $D_{\max}$ and p are specified and determine the value of γ_o.

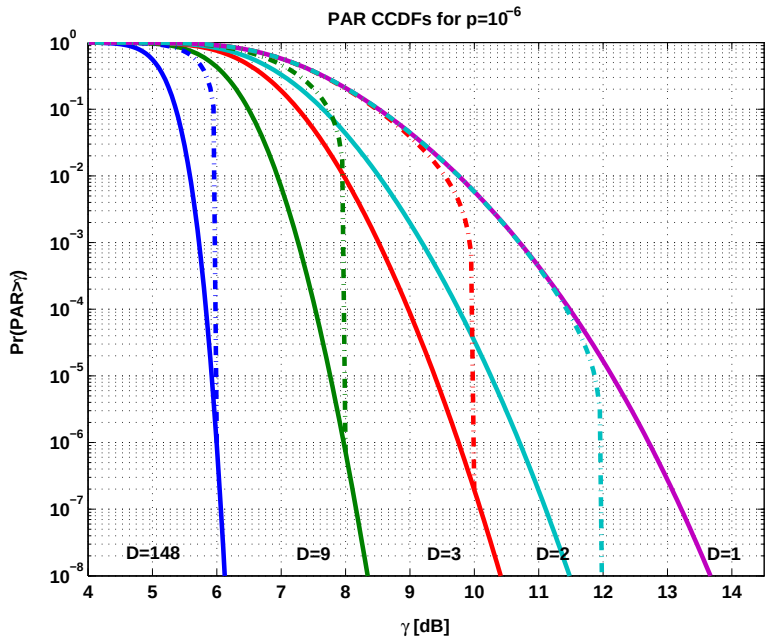

Figure 24: Different CCDFs for $\gamma_o = \{6, 8, 10, 12\}$dB and $p = 10^{-6}$. For each (γ_o, p) combination, the CCDF for traditional (solid line) as well as orderer testing (dashed line) SLM is plotted. $N = 128$.

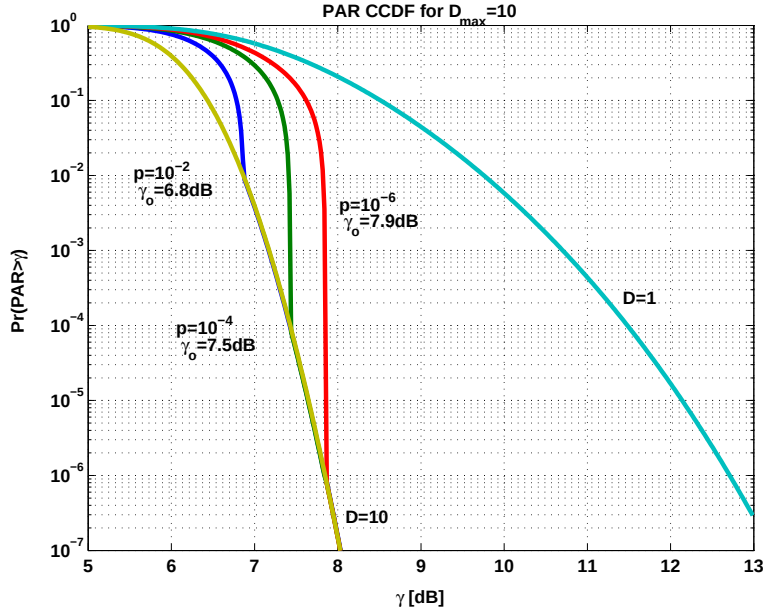

Figure 25: Different CCDFs for $D_{\max} = 10$ and $p = \{10^{-2}, 10^{-4}, 10^{-6}\}$. $N = 128$.

5.2 Threshold SLM CCDF

In deriving the CCDF of a threshold SLM OFDM symbol we were enlighten by [52]. In threshold SLM additional phase mappings are tried only if the PAR threshold, γ_o has not been met by one of the previous mappings. Thus if the d_o^{th} mapping is being tested, then the $d \in [0, d_o - 1]$ mapping all lead to PARs above the threshold. Stated mathematically,

$$Pr[PAR(\boldsymbol{x}^{(d_o)}) \leq \gamma] = Pr\left[\bigcap_{d=0}^{d_0-1} (PAR(\boldsymbol{x}^{(d)}) > \gamma_o) \text{ and } (PAR(\boldsymbol{x}^{(d_o)}) \leq \gamma)\right] \tag{83}$$

$$= \Gamma^N \left(1 - \Gamma_o^N\right)^{d_o}. \tag{84}$$

Now we have to sum over all of the possible d_os to get

$$Pr[PAR(\boldsymbol{x}^{(\tilde{d})}) \leq \gamma] = \sum_{d_o=0}^{D_{\max}-1} Pr[PAR(\boldsymbol{x}^{(d_o)}) \leq \gamma] \tag{85}$$

$$= \sum_{d_o=0}^{D_{\max}-1} \Gamma^N \left(1 - \Gamma_o^N\right)^{d_o} \tag{86}$$

$$= \frac{\Gamma^N}{\Gamma_o^N} \left(1 - (1 - \Gamma_o^N)\right)^{D_{\max}}. \tag{87}$$

If $D_{\max}$ mappings have been tried and the PAR is still above γ_o then the CCDF curve is the same as SLM with $D_{\max}$ mappings. Thus the CCDF of the PAR of a threshold SLM system is

$$Pr[PAR_{\text{tslm}} > \gamma] = \begin{cases} \frac{\Gamma^N}{\Gamma_o^N} \left(1 - (1 - \Gamma_o^N)\right)^{D_{\max}}, & \gamma \leq \gamma_o; \\ (1 - \Gamma^N)^{D_{\max}}, & \gamma > \gamma_o. \end{cases} \tag{88}$$

5.3 Mean, Variance Distribution of D

The expectation of the number, D, of independent phase sequences needed to guarantee that a given ODFM symbol has a PAR less than some level γ_o. This is important in practical applications because the transmission PA is peak-power limited, which translates to a fixed clipping level; therefore, there is no reason to further reduce the PAR of an OFDM symbol if its PAR is already low enough to avoid clipping [22]. Accordingly, any practical implementation of SLM would have some threshold PAR, γ_o, where once the signal PAR is below this level, the signal is sent without any further phase mapping. Thus, we

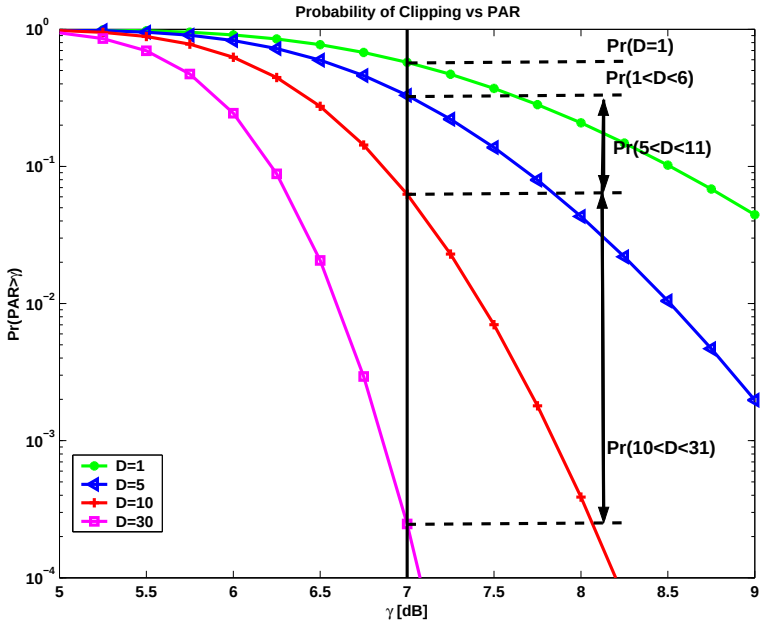

Figure 26: CCDF for $N = 128$ for various Ds. The vertical line represents the PAR value at which we guarantee no clipping occurs.

are interested in an expression for the expected number of phase mappings necessary to guarantee a certain PAR.

Figure 26 shows the PAR CCDF for $D \in [1,\ 5,\ 10,\ 30]$. The plot shows that for a γ_o of 7dB there is a 70% chance that it will be necessary to use SLM to avoid clipping. Accordingly, there is a 30% chance that we will need $D > 5$. With this understanding the distribution comes easily. If $D_{\max}$ and γ_o are known, the probability of selecting the d^{th} mapping becomes

$$\begin{aligned} \Pr(d) &= \Pr(PAR > \gamma_o)^d - \Pr(PAR > \gamma_o)^{d+1} \\ &= \begin{cases} \Gamma_o^N \left(1 - \Gamma_o^N\right)^d, & 0 \le d < D_{\max}, \\ \left(1 - \Gamma_o^N\right)^{D_{\max}}, & d = D_{\max}. \end{cases} \end{aligned} \tag{89}$$

Because the mappings are performed in the same order every time, the expression in (89) is the probability that the d^{th} phase sequence was used in transmission [8]. We will show in the next chapter how this analysis leads to an improved sequence detection performance.

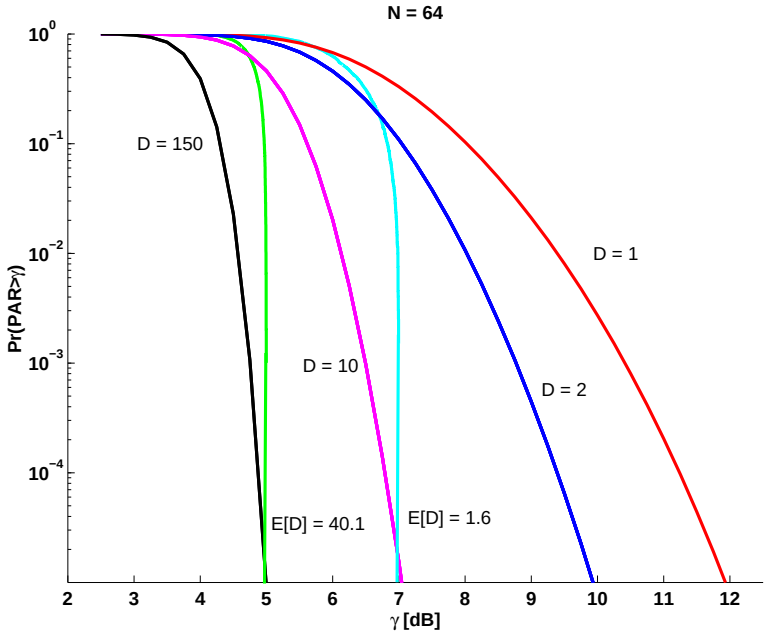

Figure 27: CCDF of the PAR for $D = 1, 2, 10, 150$. Also plotted the CCDFs for $E[D] = 1.6$ and $E[D] = 40.1$. These two CCDFs interesse the CCDF for $D = 10$ and $D = 150$ at 5dB and 7dB, respectively.

From the distribution, $E[D]$ for a general SLM scheme becomes

$$\begin{aligned} E[D] &= \Gamma_o^N \sum_{d=0}^{\infty} d\big(1-\Gamma_o^N\big)^d \\ &= \Gamma_o^{-N} \end{aligned} \tag{90}$$

and the variance in the number of mapping becomes

$$Var(D) = E[D^2] - E[D]^2 \tag{91}$$

$$= \Gamma_o^N \sum_{d=0}^{\infty} (d+1)^2 \big(1-\Gamma_o^N\big)^d - \Gamma_o^{-2N} \tag{92}$$

$$= \Gamma_o^{-2N}(1-\Gamma_o^N). \tag{93}$$

Figure 27 is a plot that demonstrates how a threshold SLM used much fewer mappings to achieve the same PAR reduction. From the plot, SLM would take 150 mapping to achieve a 5dB PAR at the 10^{-5} level. However, the expected number of mappings is only 40.1. Several values for the mean and standard deviation are listed in Table 8. Notice for this none threshold case, thus, these clipping levels are guaranteed at any probability level.

Let us explore the ratio of D to the expected D as the clipping level is lowered to a

Table 8: Several values for the mean and standard deviation in the number of mapping in a SLM system. $N = 64$.

γ_o (dB)	μ_D	σ_D
7	1.53	0.29
6	3.33	1.5
5	15.9	11.9
4	224.5	210

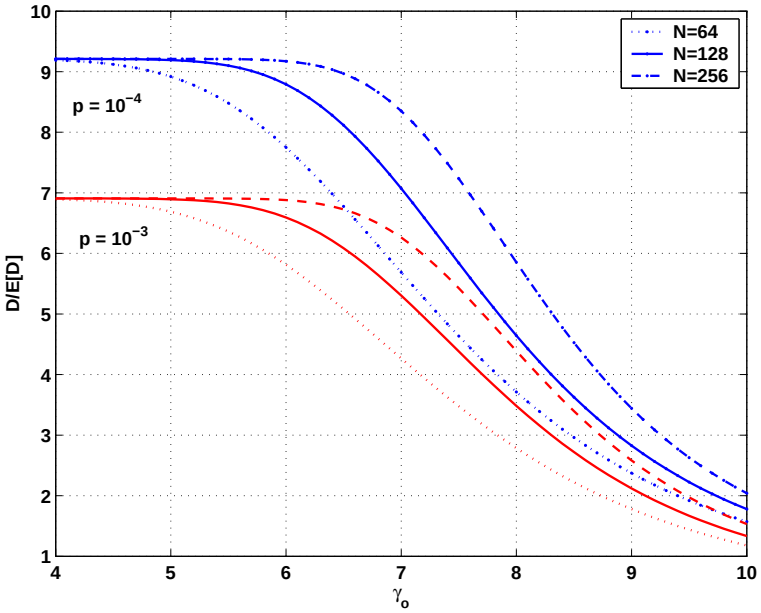

Figure 28: $D/E[D]$ versus the clipping level, γ_o. The plot is for $p = 10^{-4},\ 10^{-3}$ and $N = 64,\ 128,\ 256$.

small value such that $\Gamma_o^N \to 0$ with the limit

$$\lim_{\Gamma_o^N \to 0} \frac{D}{E[D]} = \lim_{\Gamma_o^N \to 0} \frac{\Gamma_o^N \ln(p)}{\ln(1-\Gamma_o^N)} \tag{94}$$

$$= -\ln(p), \tag{95}$$

where the expression for D is taken from (80). This limit represents the factor by which the computational complexity of SLM is reduced by implementing a PAR threshold. Figure 28 is an illustration of how quickly this limit is reached for different symbol lengths. the limit is reached much sooner for larger N. Also, several values of the limit are tabulated in Table 9.

Obviously, a practical system would not be able to evaluate for an infinite number of Ds.

Table 9: Limiting factor of computational saving by implementing a PAR threshold.

p	10^{-2}	10^{-3}	10^{-4}	10^{-5}	10^{-6}
$\lim \frac{D}{E[D]}$	4.61	6.91	9.21	11.51	13.82

Instead, a practical system would implement some type of threshold SLM. The expected number of mappings in threshold SLM is given by

$$\begin{aligned} E[D_{\text{tslm}}] &= \Gamma_o^N \sum_{d=0}^{D_{\max}-1} (d+1)\big(1-\Gamma_o^N\big)^d + D_{\max}\big(1-\Gamma_o^N\big)^{D_{\max}} \\ &= \Gamma_o^{-N}[1-(1-\Gamma_o^N)^{D_{\max}}]. \end{aligned} \tag{96}$$

In [53] a queuing scheme was presented for threshold SLM called dynamic SLM (DSLM). The scheme worked by putting a queue before and after the SLM mechanism. The output queue keeps the frequency of the sent symbols constant, while the input queue is a waiting area for symbols that have yet to be mapped. If the queues are chosen long enough then the expected number of mappings in DSLM approaches the limit set by (90).

5.4 Conclusions

In this chapter we presented threshold SLM which has a lower complexity than traditional SLM. We developed this idea by examining how a practical transmission PA is affected by PAR reduction. Next, we derived the PAR CCDF in a threshold SLM system. Finally, we derived the expected number of mapping required for SLM and demonstrated that in threshold SLM the only the $E[D]$ mappings are used on average, which is much less than the D mapping used by traditional SLM.

CHAPTER VI

BLIND SELECTED MAPPING

Blind SLM (BSLM) refers to a SLM system where the phase sequence that was used in the transmitter to minimized the PAR, $\boldsymbol{\phi}^{\tilde{d}}$, is detected in the receiver without side information. It is assumed that both the transmitter and receiver have a table of all possible phase mappings.

In this chapter will survey the BSLM methods that are in the literature. And then we will derive the maximum *a posteriori* (MAP) detection criterion, which is applicable to the threshold SLM described in Chapter 5. The MAP criterion is a general form of the maximum likelihood (ML) criterion that is applicable regular SLM.

6.1 Introduction

BSLM is appealing because side information transmission requires valuable bandwidth that could be used for sending useful information. Also, sending and recovering side information is not trivial. Simply reserving several subcarriers for side information and modulating these carriers after PAR reduction would not work. As was emphasized in the Chapter 2, the PAR is very sensitive to the data modulated on the subcarriers. Therefore, by modifying the data after PAR reduction, it is likely that peak regrowth will occur [31]. If the side information is added prior to the phase mappings, in order to avoid the peak regrowth problem, then recovering the side information becomes a non-trivial matter. However, there have been several side information assisted methods proposed, which were outlined in Section 3.1.1.

There have been several other methods that attempt to integrate non-explicit side information, coding and SLM. We refer to these as data rate reducing methods [16]. There is also a very clever method that integrates channel estimation and blind phase sequence detection [19] that we will explore. Finally, in [9] we present a BSLM technique that uses structured phase mappings to facilitate detection, which will be detailed in Chapter 7.

6.2 Blind SLM with Channel Estimation

Define a block fading channel to be one where the each successive OFDM symbol experiences a different channel response. In block fading channels it is necessary to somehow acquire the channel state information (CSI) so that the effect of the channel can be removed (according to (8)) and the error rate can be decreased. One promising way to acquire CSI is by inserting evenly spaced pilot tones in the frequency domain. This method is known as pilot tone assisted modulation (PTAM) [43].

In [19] it was demonstrated that PTAM's estimation ability was not affected by cyclic shifts of the pilot tones. That is, as long as the tones were equally spaced, PTSM worked well. It was also pointed out that the pilot tone have significantly more power in them than the information bearing tones. Thus, the pilot tones could be used as markers where they could be used to represent information. In the BSLM case, that information tells the receiver which phase mapping was used for PAR reduction. In [19] this method was dubbed blind selected pilot tone modulation (BSPTM). In Figure 29 there is an illustration of the frequency domain in BSPTM. Here the $N = 15$ and $D = 2$. The variable τ represents the offset of the first pilot tone from the zeroth subcarrier. It is important to realize that τ does not change when a phase vector is applied. Also, the receiver can detect τ with a simple comb correlator. Once τ is detected, the receiver will be able to dephase the received signal and recover the data. Moreover, the receiver can also use the pilot tones to recover the CSI, as it would in a normal PTAM OFDM scheme.

In [19], the authors showed that BSPTM has excellent detection rates. However, there is still room for other blind detection methods. One reason is that BSPTM can only distinguish between as many mapping as there are possible shifts. In the example from Figure 29, D can be at most 5. For larger D, BSPTM may have to be integrated with other methods. The second reason is that not all channel experience block fading. For static and even semi-static channels pilot tones would only be sent occasionally. For the symbols without pilot tones other BSLM detection methods need to be developed.

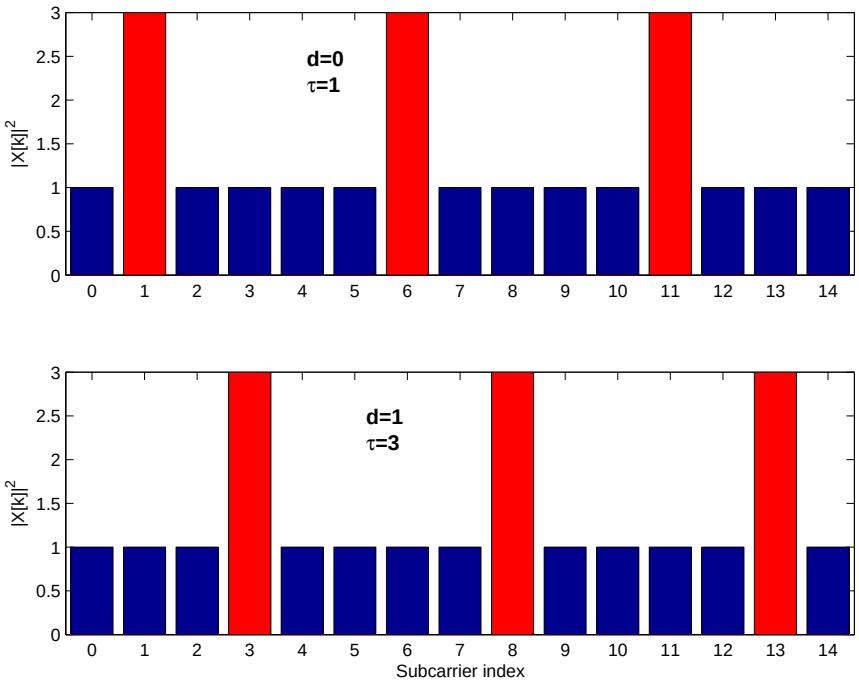

Figure 29: Example frequency domain for BSPTM with $D = 2$ and $N = 15$. The pilot tones are in red and contain more power that the information-bearing tone in blue.

6.3 Optimal BSLM Detection

In [30] a ML BSLM receiver was introduced without proof. In [9] we able to show that that receiver was actually a *suboptimal* ML receiver. In this section we will present our results from [9] and derive the MAP receiver for the threshold BSLM technique presented in Chapter 5.

6.3.1 Preliminaries

For sequence detection in BSLM it is assumed that both the transmitter and receiver have the set of possible phase sequences. The basic idea is that the receiver takes an IDFT of the received baseband signal and then uses its set of phase sequences along with some sort of metric to determine which sequence the transmitter used.

Traditionally, it is assumed that the receiver "derotates" the received symbols (as in (38)) and compares each derotation to the symbol constellation $\mathcal{C}$. However, it is convenient in the derivation of the detection metric to use a different, but equivalent, method.

Instead of derotating the received frequency-domain signal, assume that the received signal is compared to a rotated constellation. We will denote a rotated constellation sequence by $\boldsymbol{\mathcal{C}}^{(d)} = \{\mathcal{C}^{(d)}[k]\}_{k=0}^{N-1} \triangleq \mathcal{C} \cdot e^{j\boldsymbol{\varphi}^{(\tilde{d})}}$. Notice that the constellation varies with k because the phase sequence varies with k. In other words, the receiver has to determine which of the D constellation *sequences* was used for transmission. Once the constellation is known for each subcarrier (i.e. the constellation sequence is known), then classic decoding methods can be used to determine what data was sent.

6.3.2 Maximum a posteriori Probability Detection

In the following we assume an AWGN channel and an i.i.d. data sequence $\boldsymbol{X}$. With these assumptions, the maximum *a posteriori* (MAP) probability of detection is the maximum of the probability that the d^{th} constellation sequence, $\boldsymbol{\mathcal{C}}^{(d)}$, was used in transmission given the received sequence, $\mathbf{R}$. Stated mathematically,

$$\begin{aligned}
\tilde{d}^{\,(\text{MAP})} &= \underset{1\le d\le D_{\max}}{\arg\max}\ \Pr[\boldsymbol{\mathcal{C}}^{(d)}|\mathbf{R}] \\
&= \underset{1\le d\le D_{\max}}{\arg\max}\ \frac{\Pr[\mathbf{R}|\boldsymbol{\mathcal{C}}^{(d)}]\ \Pr[\boldsymbol{\mathcal{C}}^{(d)}]}{\sum_{m=1}^{D_{\max}} \Pr[\mathbf{R}|\boldsymbol{\mathcal{C}}^{(m)}]\ \Pr[\boldsymbol{\mathcal{C}}^{(m)}]} \qquad (97)\\
&= \underset{1\le d\le D_{\max}}{\arg\max}\ \Pr[\mathbf{R}|\boldsymbol{\mathcal{C}}^{(d)}]\ \Pr[\boldsymbol{\mathcal{C}}^{(d)}]. \qquad (98)
\end{aligned}$$

Note that the denominator in (97) is irrelevant because it does not depend on the maximization parameter d. If we had used the conventional derotation receiver, then the denominator would have a d dependence and would have to be included in the formulation of the metric.

In an AWGN channel the joint conditional probability density function (pdf), $f_{R[0],R[1],...,R[N-1]|\boldsymbol{\mathcal{C}}^{(d)}}(r_0, r_1, ..., r_{N-1})$, is

$$f_{\mathbf{R}|\boldsymbol{\mathcal{C}}^{(d)}}(\mathbf{r}) = \frac{1}{Q^N} \prod_{k=0}^{N-1} \sum_{q=0}^{Q-1} \frac{1}{\pi N_o} e^{-\|r[k]-\hat{c}_q^{(d)}[k]\|^2/N_o}, \qquad (99)$$

where $N_o/2$ is the noise power, $\{\hat{c}_q^{(d)}[k] \in \mathcal{C}^{(d)}[k]\}_{k=0}^{N-1}$, and $\|\cdot\|$ represents the Euclidean distance in the complex plane. We can substitute $\Pr(d)$ for $\Pr[\boldsymbol{\mathcal{C}}^{(d)}]$ and $f_{\mathbf{R}|\boldsymbol{\mathcal{C}}^{(d)}}(\mathbf{r})$ for $\Pr[\mathbf{R}|\boldsymbol{\mathcal{C}}^{(d)}]$ in (98) to obtain

$$\tilde{d}^{\,(\text{MAP})} = \underset{1\le d\le D_{\max}}{\arg\max}\ \Pr(d) \prod_{k=0}^{N-1} \sum_{q=0}^{Q-1} e^{-\|r[k]-\hat{c}_q^{(d)}[k]\|^2/N_o}, \qquad (100)$$

where $\Pr(d)$ is given in (89). Notice we were able to leave out the constant terms in $f_{\mathbf{R}|\mathcal{C}^{(d)}}(\mathbf{r})$ because of the arg max operation.

In [30] it was claimed that the optimal maximum likelihood (ML) sequence detection metric (given that the sequences are equally likely and the information modulated on each subcarrier is independent) is the minimum distance (MD) metric:

$$\tilde{d}^{\,(\mathrm{MD})} = \sum_{k=0}^{N-1} \underset{\substack{1\le d\le D_{\max}\\ 0\le q\le Q-1}}{\arg\min} \|r[k] - \hat{c}_q^{(d)}[k]\|. \tag{101}$$

In actuality that optimal ML metric is

$$\begin{aligned}\tilde{d}^{\,(\mathrm{ML})} &= \underset{1\le d\le D_{\max}}{\arg\max} \prod_{k=0}^{N-1}\sum_{q=0}^{Q-1} e^{-\|r[k]-\hat{c}_q^{(d)}[k]\|^2/N_o} \\ &= \underset{1\le d\le D_{\max}}{\arg\max} \sum_{k=0}^{N-1} \ln\left[\sum_{q=0}^{Q-1} e^{-\|r[k]-\hat{c}_q^{(d)}[k]\|^2/N_o}\right].\end{aligned} \tag{102}$$

The suboptimal metric in (101) performs almost identically to the optimal metric in (102). This is because

$$\underset{1\le d\le D_{\max}}{\arg\max}\ \ln\left[\sum_{q=0}^{Q-1} e^{-\|r[k]-\hat{c}_q^{(d)}[k]\|^2/N_o}\right] \approx \underset{\substack{1\le d\le D_{\max}\\ 0\le q\le Q-1}}{\arg\min} \|r[k] - \hat{c}_q^{(d)}[k]\|, \tag{103}$$

which is true because the constellation point used in the transmitter, $\hat{c}_{\tilde{q}}^{(\tilde{d})}[k]$, dominates the sum over Q on the left hand side of (103). This approximation is very convenient because it significantly reduces the computational complexity of the metric. Using this approximation, the suboptimal MAP (AMAP) criterion becomes

$$\tilde{d}^{\,(\mathrm{AMAP})} = \underset{1\le d\le D_{\max}}{\arg\max} \left[\ln[\Pr(d)] - \frac{1}{N_o}\sum_{k=0}^{N-1} \min_{0\le q\le Q-1} \|r[k] - \hat{c}_q^{(d)}[k]\|^2\right], \tag{104}$$

where $\Pr(d)$ is given in (89). Also, we will refer to

$$G^{(d)}(\mathbf{R}) \triangleq \ln[\Pr(d)] - \frac{1}{N_o}\sum_{k=0}^{N-1} \min_{0\le q\le Q-1} \|r[k] - \hat{c}_q^{(d)}[k]\|^2 \tag{105}$$

as the suboptimal MAP metric.

The expression in (104) requires D times as many $\|\cdot\|^2$ operations as non-SLM ML decoding. Unlike standard ML decoding, a minimum operation is necessary instead of

an argument minimum operation. Also, implementing the argument maximum operation with a threshold, while intuitively appealing, will result in a significant detection error rate (DER) increase. We will examine this effect in the next section.

6.3.3 Error Rate Analysis

The distribution of the metric $G^{(d)}(\mathbf{R})$ in an AWGN channel is complicated by the minimum operation. Instead of it being a simple non-central χ^2 (NCCS) random variable with $2N$ degrees of freedom, it is a more complicated distribution. However, for practical values of N and for large signal-to-noise ratios (SNRs) the distribution of G is closely approximated by the NCCS distribution. Note that when $d = \tilde{d}$ the distribution approaches central χ^2 (CCS). Additionally, the two distributions of $G^{(d)}(\mathbf{R})$ and $G^{(\tilde{d})}(\mathbf{R})$ are not independent because they share the same additive noise. There exists a bivariate non-central χ^2 pdf and it is given in [58]. With this pdf, $f_{G^{(d)},G^{(\tilde{d})}}(x,y)$, the phase sequence detection error rate (DER) for the d^{th} mapping is

$$DER_{d,\tilde{d}} = \int_0^\infty \int_x^\infty f_{G^{(d)},G^{(\tilde{d})}}(x,y)dydx. \tag{106}$$

The DER can be extended to the $D_{\max}$ case with

$$DER = \sum_{\tilde{d}=1}^{D_{\max}} \Pr(\tilde{d}) \sum_{\substack{d=1 \\ d\neq\tilde{d}}}^{D_{\max}} DER_{d,\tilde{d}}. \tag{107}$$

Despite the simplicity of (106) and (107), there is a complication, which is that the pdf given in [58] is not amenable to numeric integration.

As an alternative, we propose to approximate $f_{G^{(d)},G^{(\tilde{d})}}(x,y)$ with a bivariate Gaussian random variable. This method can be justified by the multivariate central limit theorem because both $G^{(d)}$ and $G^{(\tilde{d})}$ are sums of a large number of independent random variables [5]. Define

$$\begin{aligned} G^{(d)} &\sim N(\mu_x, \sigma_x) \\ G^{(\tilde{d})} &\sim N(\mu_y, \sigma_y) \\ \frac{\mathrm{Cov}(\mathrm{G^{(d)}}, \mathrm{G^{(\tilde{d})}})}{\sigma_x \sigma_y} &= \rho. \end{aligned}$$

Now,

$$DER_{d,\tilde{d}} = \int_{-\infty}^{\infty}\int_{x}^{\infty} \frac{e^{\frac{-1}{2(1-\rho^2)}\left(\frac{(x-\mu_x)^2}{\sigma_x^2} - \frac{2\rho xy}{\sigma_x\sigma_y} + \frac{(y-\mu_y)^2}{\sigma_y^2}\right)}}{2\pi\sigma_x\sigma_y\sqrt{1-\rho^2}} dydx, \tag{108}$$

however, since this has to be integrated numerically, it is preferable to find an expression for (108) that involves small finite limits of integration. Using a polar coordinate system we have

$$DER_{d,\tilde{d}} = \int_{\arctan(\frac{\sigma_y}{\sigma_x})}^{\arctan(\frac{\sigma_y}{\sigma_x})+\pi} \frac{e^{-\frac{\Delta\mu^2(1-\rho\sin(2\theta))}{2(1-\rho^2)(\sigma_x\cos(\theta)-\sigma_y\sin(\theta))^2}}}{2\pi(1-\rho\sin(2\theta))} d\theta, \tag{109}$$

where $\Delta\mu = |\mu_x - \mu_y|$.

Next, we have to find an expression for the means, variances and covariances for each D, N, and γ_o. Our approach is to ignore the minimum operation in the metric to derive these statistical measures and then use simulation results that implement the minimum operation to refine the analytical expressions.

We need to find the statistical properties of the metric when $d = \tilde{d}$ and when $d \neq \tilde{d}$. For a Q-ary PSK constellation with constellation points at angles $\{\phi_q\}_{q=0}^{Q-1}$ and magnitude $\sqrt{E_s}$ we have

$$E[G^{(d\neq\tilde{d})}] = -N - 2N\frac{E_s}{N_o}\left(1 - \frac{Q}{\pi}\sin(\frac{\pi}{Q})\right) + \ln[\Pr(D=d)] \tag{110}$$

$$Var[G^{(d\neq\tilde{d})}] = N + 2N\frac{E_s^2}{N_o^2}\left(1 + \frac{Q}{\pi}\sin(\frac{\pi}{Q})\cos(\frac{\pi}{Q}) - \frac{2Q^2}{\pi^2}\sin^2(\frac{\pi}{Q})\right) \tag{111}$$

$$E[G^{(\tilde{d})}] = -N + \ln[\Pr(D=\tilde{d})] \tag{112}$$

$$Var[G^{(\tilde{d})}] = N \tag{113}$$

$$Cov[G^{(\tilde{d})}, G^{(d)}] = N. \tag{114}$$

where the phase angles in the phase mappings are uniformly distributed on $[0, 2\pi)$ (see appendix for details). These equations are appealing because they can be expressed in a relatively simple closed form. On the other hand, they are of limited use in that they are only applicable to PSK constellations. DSL systems use very large QAM constellations [59] which are not amenable to the the sort of closed form analysis we were able to provide for PSK constellations.

Using the Gaussian error rate approximation on statistical measures derived through simulations is far easier and less time consuming than full simulations. This is because we only have to run one simulation per constellation for a range of SNRs. Because mean, variance and covariance are linear in N, it is straightforward to extrapolate these measures for any N. Furthermore, any change in $D_{\max}$ just changes the means for the metric by a known value and adds an extra term to the summation in (107). Accordingly, we have provided the best-fit lines for the statistical measures in Table 10.

Table 10: Statistical measures for different constellations based on a best fit analysis.

4-QAM

$\Delta\mu$	$\ln[\cosh(0.2224\frac{E_s}{N_o})]$
σ_x^2	$0.03076\frac{E_s^2}{N_o^2} + 0.0581\frac{E_s}{N_o} + 0.53$
σ_y^2	$1.00 - 0.4\exp(-0.04\frac{E_s^2}{N_o^2})$
$Cov[X,Y]$	0.50

16-QAM

$\Delta\mu$	$\ln[\cosh(0.0639\frac{E_s}{N_o})]$
σ_x^2	$0.00305\frac{E_s^2}{N_o^2} + 0.0366\frac{E_s}{N_o} + 0.31$
σ_y^2	$1.00 - 0.7\exp(-3.2\times10^{-3}\frac{E_s^2}{N_o^2})$
$Cov[X,Y]$	0.29

64-QAM

$\Delta\mu$	$\ln[\cosh(0.022\frac{E_s}{N_o})]$
σ_x^2	$9.5\times10^{-4}\frac{E_s^2}{N_o^2} + 0.023\frac{E_s}{N_o} + 0.195$
σ_y^2	$1.00 - 0.84\exp(-8\times10^{-5}\frac{E_s^2}{N_o^2})$
$Cov[X,Y]$	0.21

256-QAM

$\Delta\mu$	$\ln[\cosh(0.00904\frac{E_s}{N_o})]$
σ_x^2	$4.6\times10^{-4}\frac{E_s^2}{N_o^2} + 0.026\frac{E_s}{N_o} + 0.085$
σ_y^2	$1.00 - 0.91\exp(-5.2\times10^{-6}\frac{E_s^2}{N_o^2})$
$Cov[X,Y]$	0.18

Figure 30 is a plot of the DER using the Gaussian approximation and the parameters from Table 1. There is a curve for each constellation and for the ML and MAP metrics.

The PAR reduction parameters used for the plot are $N = 512$, $\gamma_o = 10$ dB, $p = 10^{-7}$ and $D_{\max} = 5$ which is a 3.5 dB PAR reduction. The plot shows that by using the MAP metric, we can achieve an order of magnitude improvement in the DER. Note that this improvement is gained with negligible complexity increase ($D_{\max}$ extra additions). Figure 31 is a DER plot with parameters $N = 1024$, $\gamma_o = 9$ dB, $p = 10^{-7}$ and $D_{\max} = 14$, which is a 4.5 dB PAR reduction. The plot shows that the DER is lower even though more mappings were used, which is due to the increase in the number of subcarriers. The effect of N on the DER is illustrated more clearly in Figure 32 where the DER with $E_b/N_o = 7$ dB is plotted against N. We can see that the DER decreases exponentially with N when the number of mappings is held constant.

Figure 33 is a plot of the bit error rate (BER) in an AWGN channel with a hard limiter 10 dB above the average signal power. The plot illustrates how different coding gains can affect the BER in a BSLM system. For the uncoded case the BER is dominated by errors in constellation point detection which means that the ML and MAP curves coincide. The OFDM without SLM curve is higher because of clipping errors incurred by the hard limiter. When a coding gain of 6 dB is used we can see a distinct difference between the three curves. Specifically, we can see that the MAP criterion has about a 0.8 dB advantage over the ML criterion at the 10^{-6} BER level.

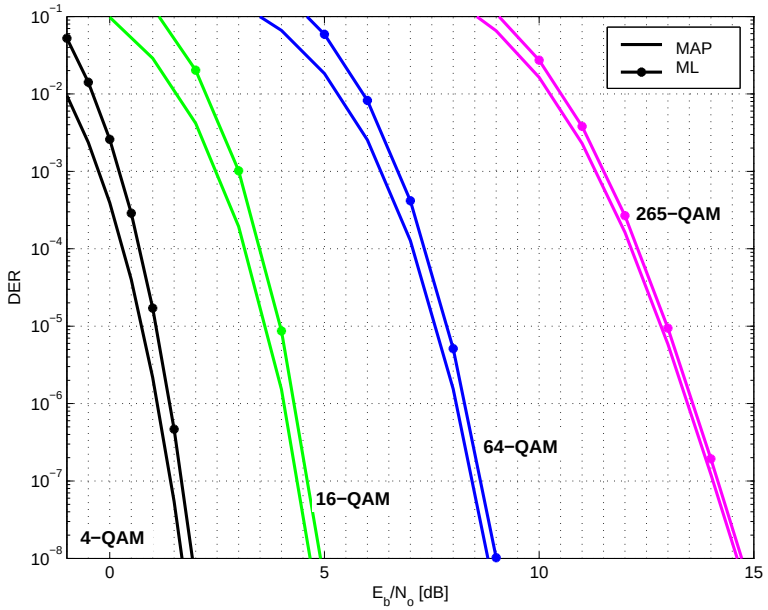

Figure 30: Plot parameters: $N = 512$, $\gamma_o = 10$ dB, $p = 10^{-7}$ and $D_{\max} = 5$. The DER is plotted versus the bit energy to noise ratio for different constellations. For each constellation, the DER for the suboptimal ML (starred) and MAP (line) detection methods are plotted.

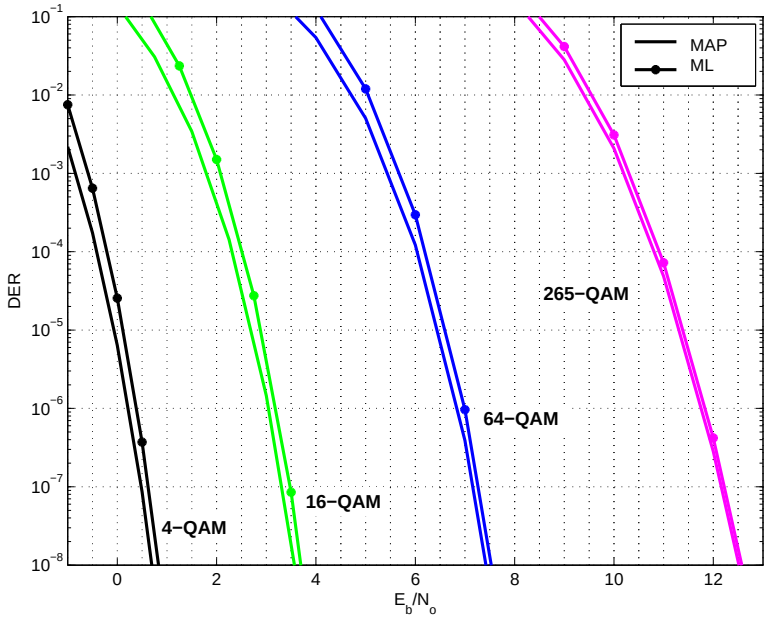

Figure 31: Plot parameters: $N = 1024$, $\gamma_o = 9$ dB, $p = 10^{-7}$ and $D_{\max} = 14$. The DER is plotted versus the bit energy to noise ratio for different constellations. For each constellation, the DER for the suboptimal ML (starred) and MAP (line) detection methods are plotted.

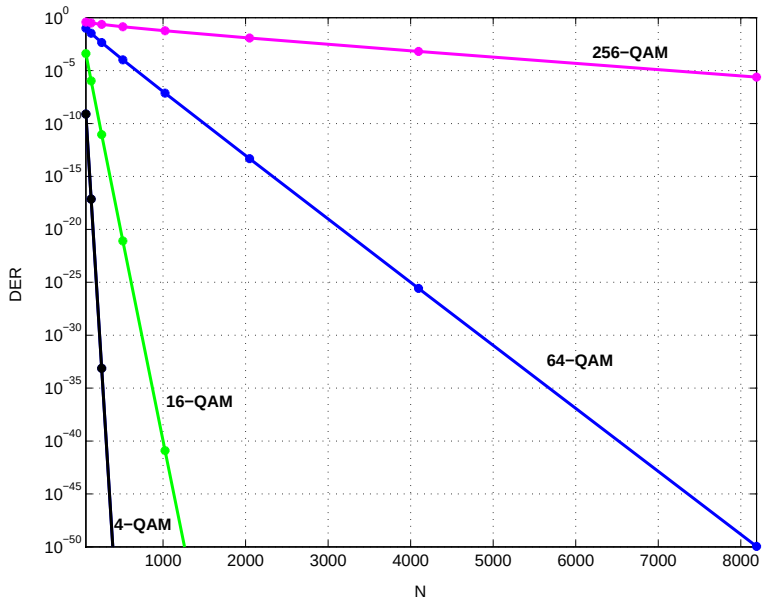

Figure 32: Plot parameters: $E_b/N_o = 7$ dB and $D_{\max} = 5$. The DER is plotted versus the number of subcarriers, N.

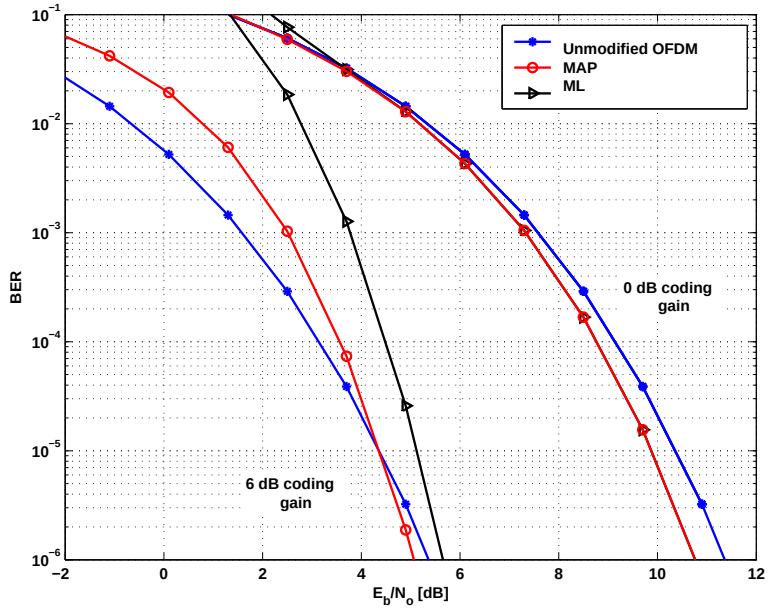

Figure 33: Bit error rate plot for BSLM in an AWGN channel with a hard limiter and 4-QAM modulation. The leftmost set of lines correspond to a system with a 6 dB coding gain, while the lines on the right correspond to the uncoded case. For each case there is a plot of BER for the unmodified OFDM, detection with the ML criterion, and detection with the MAP criterion. Plot parameters: $N = 64$, $\gamma_o = 10$ dB, $p = 10^{-7}$ and $D_{\max} = 3$.

6.4 Conclusions

In this chapter we have presented an outline of several BSLM detection techniques that are in the literature. Additionally, we derived the MAP criterion for detecting phase sequences in BSLM. In deriving this MAP criterion it was necessary to define several details about the how the transmitter and receiver operate. Specifically, the transmitter only uses as many mappings as necessary to get below the clipping level (i.e. threshold SLM is used), and the receiver compares the received symbols to a rotated constellation. The first specification ensures that each mapping has a different probability, while the second allows for a simplified MAP metric.

6.5 Derivation of the Mean, Variance and Covariance of $G^{(d)}$ in PSK Constellations

Here we assume an AWGN channel and a PSK constellation with constellation points at angles $\{\phi_q\}_{q=0}^{Q-1}$. First define the noise pdf to be

$$g_{X,Y}(x,y) \triangleq \frac{1}{N_o\pi} e^{\frac{-1}{N_o}(x^2+y^2)}. \tag{115}$$

Now, when the incorrect constellation is used in the metric (i.e. $d \neq \tilde{d}$) and the possible mapped phase angles are uniformly distributed on $[0, 2\pi)$, we can view the transmitted points as being uniformly distributed on $[0, 2\pi)$ with power of E_s. Thus, to calculate the expected value of $G^{(d\neq\tilde{d})}$ we must find the expected squared distance between the constellation points, $\sqrt{E_s}\{\cos(\phi_q) + \sin(\phi_q)\}_{q=0}^{Q-1}$, and a point that is uniformly distributed around the circle with modulus $\sqrt{E_s}$ that has been corrupted with additive noise. Additionally, we have to add $\ln[\Pr(d)]$ to the mean because it is a MAP metric. Finally, notice in (105) that

$G^{(d)}$ has a factor of $1/N_o$ in it. The expected value when $d \neq \tilde{d}$ is

$$\begin{aligned}
E[G^{(d)}] =& \frac{-N}{2\pi N_o} \sum_{q=0}^{Q-1} \int_{\phi_q-\pi/Q}^{\phi_q+\pi/Q} \int_{-\infty}^{\infty} \int_{-\infty}^{\infty} \left((x + \sqrt{E_s}(\cos(\theta) - \cos(\phi_q)))^2 \right. \\
& \left. + (y + \sqrt{E_s}(\sin(\theta) - \sin(\phi_q)))^2\right) g_{X,Y}(x,y) dy dx d\theta + \ln[\Pr(D = d)] \\
=& -N - N\frac{E_s}{2\pi N_o} \sum_{q=0}^{Q-1} \int_{\phi_q-\pi/Q}^{\phi_q+\pi/Q} (\cos(\theta) - \cos(\phi_q))^2 + (\sin(\theta) - \sin(\phi_q))^2 d\theta \\
& + \ln[\Pr(D = d)] \\
=& -N - 2N\frac{E_s}{N_o}\left(1 - \frac{Q}{\pi}\sin(\frac{\pi}{Q})\right) + \ln[\Pr(D = d)]. \qquad (116)
\end{aligned}$$

When $d \neq \tilde{d}$ the variance can be calculated by

$$\begin{aligned}
E[(G^{(d)} - \ln[\Pr(d)])^2 | N = 1] =& \frac{1}{2\pi N_o^2} \sum_{q=0}^{Q-1} \int_{\phi_q-\pi/Q}^{\phi_q+\pi/Q} \int_{-\infty}^{\infty} \int_{-\infty}^{\infty} \left((x + \sqrt{E_s}(\cos(\theta) - \cos(\phi_q)))^2 \right. \\
& \left. + (y + \sqrt{E_s}(\sin(\theta) - \sin(\phi_q)))^2\right)^2 g_{X,Y}(x,y) dy dx d\theta \\
=& 2 + \frac{E_s}{N_o}\ 4\left(1 - \frac{Q}{\pi}\sin(\frac{\pi}{Q})\right) \\
& + \frac{E_s^2}{N_o^2}\ 2\left(3 + \frac{Q}{\pi}\sin(\frac{\pi}{Q})\cos(\frac{\pi}{Q}) - \frac{4Q}{\pi}\sin(\frac{\pi}{Q})\right) \\
Var[G^{(d)}] =& N + N\frac{E_s^2}{N_o^2}\left(2 + \frac{2Q}{\pi}\sin(\frac{\pi}{Q})\cos(\frac{\pi}{Q}) - \frac{4Q^2}{\pi^2}\sin^2(\frac{\pi}{Q})\right). \qquad (117)
\end{aligned}$$

When $d = \tilde{d}$ the calculations are much easier because it is just the mean and variance of a central χ^2 random variable with two degrees of freedom:

$$\begin{aligned}
E[G^{(\tilde{d})}] =& \frac{-N}{N_o} \int_{-\infty}^{\infty} \int_{-\infty}^{\infty} \left(x^2 + y^2\right)\ g_{X,Y}(x,y) dx dx + \ln[\Pr(\tilde{d})] \\
=& -N + \ln[\Pr(\tilde{d})] \qquad (118) \\
E[(G^{(\tilde{d})} - \ln[\Pr(\tilde{d})])^2 | N = 1] =& \frac{1}{N_o^2} \int_{-\infty}^{\infty} \int_{-\infty}^{\infty} \left(x^2 + y^2\right)^2\ g_{X,Y}(x,y) dx dx \\
=& 2 \\
Var[G^{(\tilde{d})}] =& N. \qquad (119)
\end{aligned}$$

Lastly, the covariance between $G^{(\tilde{d})}$ and $G^{(d)}$ is

$$\begin{aligned}
E[(G^{(d)} - \ln[\Pr(d)])(G^{(\tilde{d})} - \ln[\Pr(\tilde{d})])|N=1] = \\
&\frac{1}{2\pi N_o^2} \sum_{q=0}^{Q-1} \int_{\phi_q - \pi/Q}^{\phi_q + \pi/Q} \int_{-\infty}^{\infty} \int_{-\infty}^{\infty} \big((x + \sqrt{E_s}(\cos(\theta) - \cos(\phi_q)))^2 \\
&\quad + (y + \sqrt{E_s}(\sin(\theta) - \sin(\phi_q)))^2\big)\left(x^2 + y^2\right)\, g_{X,Y}(x,y) dy dx d\theta \\
&= 2 + 2\frac{E_s}{N_o}\left(1 - \frac{Q}{\pi}\sin(\frac{\pi}{Q})\right) \\
Cov[G^{(\tilde{d})}, G^{(d)}] &= N. \qquad (120)
\end{aligned}$$

CHAPTER VII

MONOMIAL PHASE SEQUENCES FOR BLIND SELECTED MAPPING DETECTION

In the previous chapter we presented several blind SLM detection methods, including the optimal MAP detection. In this chapter we will present work from [11], where it was demonstrated that monomial phase sequences can be detected with the complexity of a single FFT in the receiver. This is a significant improvement of MAP detection which has a complexity proportional to the number of mappings. Of course, there is a tradeoff in BER for this complexity improvement that will have to be considered before implementation.

7.1 Monomial Phase Sequence SLM

It has been shown in [69] that it is possible to use phase sequences of the form $\phi_k^{(d)} = \alpha^{(d)} k^p \equiv ((\alpha^{(d)} k^p))_{2\pi}$[1] in SLM and still achieve almost optimal PAR-reduction performance. Here $\alpha^{(d)}$ is some constant. The idea is that for $p > 1$, $\phi_k^{(d)} \sim U[0, 2\pi)$, thus the independence condition that $E[e^{j\phi_k^{(d)}}] = 0$ is (approximately) satisfied.

However, $((\alpha^{(d)} k^p))_{2\pi}$ must also be (approximately) i.i.d. across all ds and ks. In other words, $((\alpha^{(d)} k^p))_{2\pi}$ needs to be aperiodic in both k and d. The simplest way to guarantee aperiodicity is to set α so that it is *not* a multiple of π. It is possible to achieve near optimum PAR reduction performance, even when α is a multiple of π, by making the period $\alpha^{(d)} k^p \mod 2\pi$ in k larger than N and making the period in d larger than D.

Figure 34 is a plot that compares the PAR reduction capability of monomial phase sequences to randomly generated phase sequences. In the plot QPSK is used for modulation, $N = 64$, $D = 10$, the monomial exponents are $p = 2, 3$, $\alpha^{(d)}$ is chosen according to the description in the next section, and the random phase sequence is uniformly distributed: $\phi \sim U(0, 2\pi]$. The CCDF for each phase sequence is plotted for the Nyquist-sampled case

[1] $((\cdot))_N$ represents the modulo N of teh argument

($L = 1$) as well as the $L = 4$ case. The plot shows that all three phase sequences have virtually identical PAR-reduction performance for either oversampling factor. The $p = 2$ case has a slightly larger CCDF tail than the other mappings, but this should be a negligible difference in most applications.

7.2 Blind Detection of Monomial Phase Sequences

If the phase sequences are monomials in k and we have some way to nullify the data, then detecting $\alpha^{(\tilde{d})}$ or, equivalently, $\tilde{d}$, becomes a polynomial phase estimation problem. This problem has been well studied in the context of doppler radar and wireless communications applications.

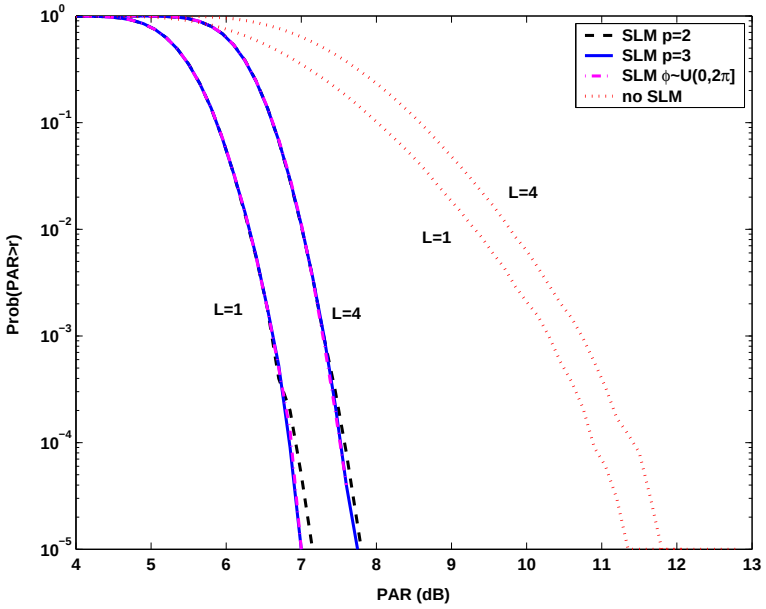

Figure 34: CCDF of SLM and monomial SLM, with $N = 64$ and $D = 10$ phase mappings. Both, the $L = 1$ and $L = 4$ cases are plotted.

If a M-PSK constellation is used, and the received frequency domain signal, $Y_k^{(\tilde{d})}$, is raised to the M^{th} power, then the effect of the data is nullified. For instance, if X_k is drawn from a QPSK constellation ($\{-1, 1, -j, j\}$), then $X_k^4 = 1$ regardless of which QPSK constellation point is used. In general, for M-PSK and monomial phase sequences, we have

$$(Y_k^{(\tilde{d})})^M = e^{jM\alpha^{(\tilde{d})}k^p} \triangleq W_k. \tag{121}$$

Here, W_k is a monomial phase complex exponential of order p. The peaks of power spectrum

can be used to estimate the α parameter. To do this, a signal that is a complex exponential with linear (or affine) phase in k, with α as one of the factors of the linear coefficient must be created. For example, assume $M = 2$ (BPSK) and $p = 2$. Examine

$$W_k W_{k-1}^* = e^{j2\alpha^{(\tilde{d})}k^2} e^{-j2\alpha^{(\tilde{d})}(k-1)^2} \tag{122}$$

$$= e^{j2\alpha^{(\tilde{d})}k^2 - j2\alpha^{(\tilde{d})}(k-1)^2} \tag{123}$$

$$= e^{j4\alpha^{(\tilde{d})}k - j2\alpha^{(\tilde{d})}}. \tag{124}$$

The DFT of the product $W_k W_{k-1}^*$, where $k \in [1, N-1]$, has a peak at the sample closest to $\frac{(N-1)4\alpha^{(\tilde{d})}}{2\pi}$. The formula can be generalized for any p.

Define

$$V_q \triangleq \left[\prod_{\substack{i=0 \\ i \text{ even}}}^{p-1} \left(W_{q-i}\right)^{\binom{p-1}{i}} \right] \left[\prod_{\substack{l=1 \\ l \text{ odd}}}^{p-1} \left(W_{q-l}^*\right)^{\binom{p-1}{l}} \right], \tag{125}$$

where $q \in [p-1, N-1]$. For convenience, assume that V_q is zero-padded so that it is length N, (i.e. $\{V_q\}_{q=0}^{p-2} = 0$). It can be shown that

$$\hat{\alpha}^{(\tilde{d})} = \frac{2\pi}{N\ M\ p!} \underset{0 \le n < N}{\text{argmax}} \left| \sum_{q=0}^{N-1} V_q e^{\frac{j2\pi qn}{N}} \right| \tag{126}$$

is an unbiased estimator when W_k is in the presence of additive white noise [70]. Also, notice that the Nyquist-sampled DFT is used to estimate α. Traditionally, in polynomial phase detection problems, it is necessary to find a precise estimate for the polynomial phase coefficients, which is done with an oversampled DFT and interpolation methods [72]. However, in the context of blind SLM detection, there are a finite number ($D << N$) of possible coefficients. Thus, using an oversampled DFT would increase the complexity without increasing the detection performance.

The right hand side (RHS) of (126) is π times a rational number. In the interest of detecting $\alpha^{(d)}$ it is natural to want to choose multiples of $\frac{N\ M\ p!}{2\pi}$ for $\alpha^{(d)}$ so that $\hat{\alpha}^{(\tilde{d})}$ will fall neatly into the DFT grid. However, in the interest of minimizing the PAR, $\alpha^{(d)}$ needs to satisfy a contradictory condition. As mentioned in Section IV, $\phi_k^{(d)} \mod 2\pi$ needs to be aperiodic in k and d. If $\alpha^{(d)} \in \mathbb{Q}$, then ϕ will be aperiodic, but

$$E\left[\underset{0 \le n < N}{\text{argmax}} \left| \sum_{q=0}^{N-1} V_q e^{\frac{j2\pi qn}{N}} \right| \right] = \alpha^{(\tilde{d})} \frac{N\ M\ p!}{2\pi} \notin \mathbb{Q}, \tag{127}$$

which is undesirable because because it makes partitioning the DFT beams into D equal-sized equiprobable bins impossible.

In order to strike a balance between PAR-reduction performance and detection capability, we propose that $\{\alpha^{(d)}\}_{d=0}^{D-1} = \frac{6.3\ d}{D\ M\ p!}$. In this case, the DFT grid can be partitioned into D detection bins with borders given by $\frac{6.3}{2\pi}\{\frac{N}{2D},\ \frac{3N}{2D}, ...,\ \frac{(D-1)N}{D} + \frac{N}{2D}\}$. That is, $\tilde{d}$ is estimated by

$$\left(\left(\frac{6.3(2\tilde{d}-1)N}{4\pi D}\right)\right)_N \quad < \quad \underset{0\le n<N}{\text{argmax}}\left|\sum_{q=0}^{N-1} V_q e^{\frac{j2\pi qn}{N}}\right| \quad < \quad \left(\left(\frac{6.3(2\tilde{d}+1)N}{4\pi D}\right)\right)_N, \quad (128)$$

where $((\cdot))_N$ represent the modulo N of the argument.

7.3 Simulations

Figure 35 is a plot of the $\tilde{d}$-detection error rate (DER) of the monomial SLM for BPSK and QPSK constellations and $D = 10$. When QPSK is used the received signal has to be raised to the forth power according to (121), as opposed to the second power for BPSK. In an AWGN channel the additional squaring causes the DER for QPSK to be higher that the DER for BPSK.

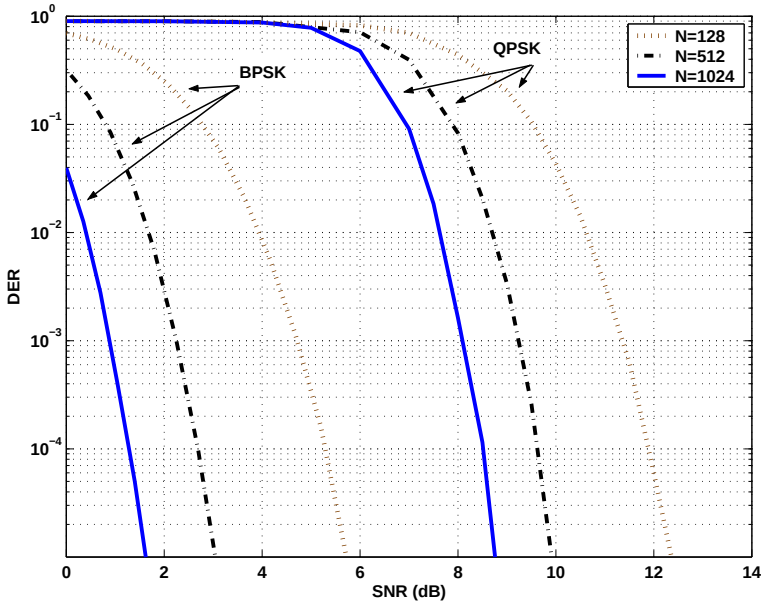

Figure 35: Detection error rate (DER) of blindly detected monomial SLM for $D = 10$ with BPSK and QPSK constellations.

Figure 36 is a plot of the bit error rate (BER) for blindly detected monomial SLM.

In order to adequately compare the BER of a high-PAR signal to the BER of a PAR-reduced signal it is appropriate to examine the the traditional SNR multiplied by the PAR at some probability level .We refer to this SNR measure as the peak signal to noise ratio (PSNR). Here, we chose $\Pr(PAR > \gamma) = 10^{-3}$, which means for $L = 4$, $\gamma_{\text{SLM}} \approx 7.5$ and $\gamma_{\text{noSLM}} \approx 10.9$.

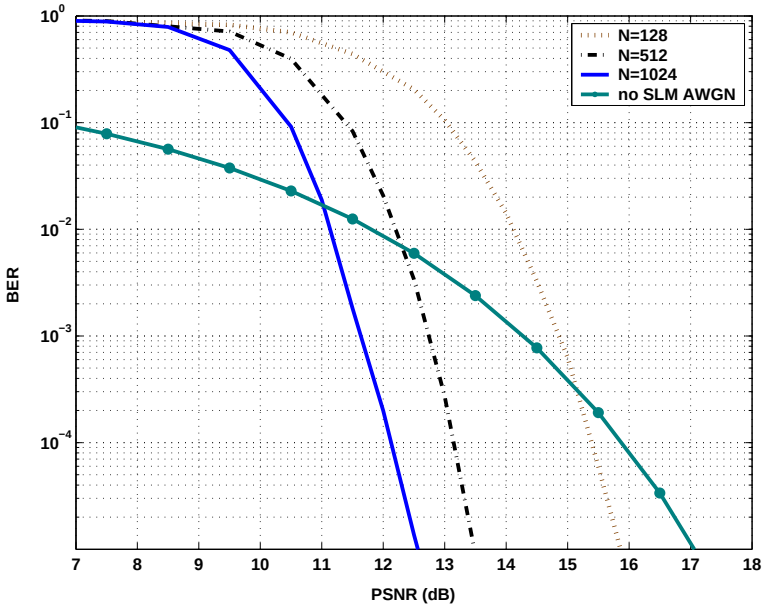

Figure 36: BER of blindly detected monomial SLM when QPSK is used compared to BER of QPSK OFDM with no SLM.

7.4 Conclusions

In this chapter we have presented a method for blind detection monomial phase sequences in a SLM OFDM system. We were able to show that a second-order monomial phase sequence allows excellent detection performance, while achieving near-optimal PAR reductions. When taken as a whole, a blindly detected monomial SLM OFDM system exhibits a significant BER improvement over non-SLM OFDM.

CHAPTER VIII

CONTRIBUTIONS AND FUTURE WORK

8.1 Contributions of this Thesis

In this thesis we have given an overview PAR reduction schemes with an emphasis on SLM in OFDM communications systems. Included in this overview, were several novel proposals for improved SLM systems. The list below summarizes the contributions of this thesis.

- We analyzed the PAR in SLM and in OFDM and were able to show that the expected PAR of OFDM or SLM can be expressed in a closed form expression.
- We demonstrated that SLM is capable of a large (several Watts) net power savings through a rigorous computational complexity analysis of a wireless communications system.
- We presented threshold SLM, which is less computationally complex than traditional SLM. We were able to quantify this reduction in complexity by deriving the expected number of mappings required for a threshold SLM system.
- We derived the optimal MAP and ML receivers and were able to show that a previously claimed optimal ML receiver ([30]) was, in fact, suboptimal.
- We demonstrated that by using monomial phase sequences, SLM receivers could perform blind phase sequence detection at a very low computational cost.

8.2 Future Work

Despite all of the attention that PAR reduction has garnered, it remains a fruit field of research. Below we list possible research topics related to the content of this thesis.

- As detailed in Section 3.1.2, selecting the minimum PAR sequence based from the Nyquist-sampled symbols results in some peak regrowth after oversampling. On the

other hand, basing selection on the oversampled symbols incurs additional computational costs. Thus, we feel that a thorough analysis of this tradeoff is in order so that the optimal balance can be determined.

- In [38] an interesting variation on SLM was proposed, where selection was based on the clipping noise power instead of PAR. We feel that this can be an extremely fruitful line of research. And currently, we are in the process of deriving the clipping noise power CCDF of OFDM symbols.

- In addition to the clipping noise power CCDF, almost all of the analysis from this thesis can be applied to the clipping noise selection scheme in [38]. Such as the expected clipping noise power in terms of the number of mappings, blind sequence detection performance analysis (which is complicated by the clipping) and the expected number of mappings to achieve a clipping noise power at a certain probability level.

- Finally, With the clipping noise CCDF, it should be possible to give a concrete analysis of the spectral regrowth cause by a clipping noise selection scheme.

REFERENCES

[1] "Operation within the bands 902-928 MHz, 2400-2483.5 MHz, and 5725-5850 MHz." Code of Federal Regulations, Title 47, Volume 1, Section 15.247, Oct. 2002.

[2] "IEEE standard local and metropolitan area network." IEEE Std. 802.16a, 2003.

[3] "DSP platforms : C5000 DSPs." http://dspvillage.ti.com/, 2004.

[4] Abouda, A. A., "PAPR reduction of OFDM signal using turbo coding and selective mapping," *Proceedings of the 6th Nordic Signal Processing Symposium*, pp. 248 – 251, June 2004.

[5] Adams, W., *The Life and Times of the Central Limit Theorem*. Kaedmon Publishing Company, 1974.

[6] Armstrong, J., "Analysis of new and existing methods of reducing intercarrier interference due to carrier frequency offset in OFDM," *IEEE Trans. Communications*, vol. 47, pp. 365 – 369, Mar. 1999.

[7] Bauml, R., Fischer, R., and Huber, J., "Reducing the peak-to-average power ratio of multicarrier modulation by selected mapping," *IEE Electronics Letters*, vol. 32, pp. 2056–2057, Oct. 1996.

[8] Baxley, R. J. and Zhou, G. T., "Assessing peak-to-average power ratios for communications applications," *Proc. IEEE MILCOM Conference*, Oct. 2004.

[9] Baxley, R. J. and Zhou, G. T., "MAP metric for blind phase sequence detection in selected mapping." Submitted to *IEEE Trans. on Broadcasting*, Dec. 2004.

[10] Baxley, R. J. and Zhou, G. T., "Power savings analysis of peak-to-average power ratio reduction in OFDM," *IEEE Trans. on Consumer Electronics*, vol. 50, pp. 792–798, Aug. 2004.

[11] Baxley, R. J. and Zhou, G. T., "Blind selected mapping using monomial phase sequences." To be submitted, 2005.

[12] Baxley, R. J. and Zhou, G. T., "Ordered phase sequence testing in SLM for improved blind detection." Submitted to IEEE SPAWC 2005 conference, 2005.

[13] Braithwaite, R. N., "Exploiting data and code interactions to reduce the power variance for CDMA sequences," *IEEE Journal on Selected Areas in Communications*, vol. 19, pp. 1061–1069, June 2001.

[14] Breiling, M., Muller-Weinfurtner, S. H., and Huber, J. B., "SLM peak-power reduction without explicit side information," *IEEE Communications Letters*, vol. 5, pp. 239–241, June 2001.

[15] Brillinger, D., *Time Series Data Analysis and Theory.* Philadelphia, PA: SIAM, 2001.

[16] Carson, N. and Gulliver, A., "Peak-to-average power ratio reduction of OFDM using repeat-accumulate codes and selective mapping," *Proc. ISIT 2002*, p. 214, July 2002.

[17] Chang, R. W., "Synthesis of band-limited orthogonal signals for multichannel data transmission," *Bell Syst. Tech. J.*, vol. 45, pp. 1775–1796, Dec. 1966.

[18] Chang, R. W., "Orthogonal frequency division multiplexing." U.S. Patent 3 488 445, Jan. 1970.

[19] Chen, N. and Zhou, G. T., "Peak-to-average power ratio reduction in OFDM with blind selected pilot tone modulation," *Proc. IEEE Intl. Conference on Acoustics, Speech, and Signal Processing*, Mar. 2005.

[20] Cimini, L. J. and Sollenberger, N. R., "Peak-to-average power ratio reduction of an OFDM signal using partial transmit sequences," *IEEE Comm. Letters*, vol. 4, pp. 86 – 88, Mar. 1991.

[21] Combettes, F. L., "The foundations of set theoretic estimation," *Proceedings of the IEEE*, vol. 81, pp. 182 – 208, Feb. 1993.

[22] Cripps, S. C., *RF Power Amplifiers for Wireless Communications.* Norwood, MA: Artech House, 1999.

[23] Dinur, N. and Wulich, D., "Peak-toaverage power ratio in high-order OFDM," *IEEE Trans. Communications*, vol. 49, pp. 1063–1072, June 2001.

[24] Eevelt, P., Wade, M., and Tomlinson, M., "Peak to average power reduction for OFDM schemes by selective scrambling," *IEE Electronics Letters*, vol. 32, pp. 1963–1964, Oct. 1996.

[25] Feng, C.-C., Wang, C.-Y., Lin, C.-Y., and Hung, Y.-H., "Protection and transmission of side information for peak-to-average power ratio reduction of an OFDM signal using partial transmit sequences," *IEEE Proc. Vehicular Technology Conference*, vol. 4, pp. 2461 – 2465, Oct. 2003.

[26] Gatherer, A. and Polley, M., "Controlling clipping probability in DMT transmission," *Asilomar Conference record*, vol. 1, pp. 578 – 584, Nov. 1997.

[27] Hayes, M. H., *Statistical Digital Signal Processing and Modeling.* New York, NY: John Wiley & Sons, 1996.

[28] Ho, W. S., Madhukumar, A. S., and Chin, F., "A novel two-layered suboptimal approach to partial transmit sequences," *Proc. IEEE Vehicular Technology Conference*, vol. 2, pp. 1268 – 1272, Apr. 2003.

[29] Jayalath, A. D. S. and Tellambura, C., "Peak-to-average power ratio reduction of an OFDM signal using data permutation with embedded side information," *IEEE International Symposium on Circuits and Systems*, vol. 4, pp. 562 – 565, May 2001.

[30] Jayalath, A. D. S. and Tellambura, C., "Blind SLM receiver for PAR-reduced OFDM," *Proc. IEEE Vehicular Technology Conference*, pp. 219–222, Sept. 2002.

[31] Jayalath, A. D. S. and Tellambura, C., "Side information in PAR reduced PTS-OFDM signals," *Personal, Indoor and Mobile Radio Communications conference*, vol. 1, pp. 226 – 230, Sept. 2003.

[32] Jayalath, A. and Athaudage, C., "On the PAR reduction of OFDM signals using multiple signal representation," *IEEE Communications Letters*, vol. 8, pp. 425 – 427, July 2004.

[33] Jones, A. E., Wilkinson, T. A., and Barton, S. K., "Block coding scheme for reduction of peak to mean envelope power ratio of multicarrier transmission schemes," *IEE Electronics Letters*, vol. 30, pp. 2098 – 2099, Dec. 1994.

[34] Kang, S. G., Kim, J. G., and Joo, E. K., "A novel subblock partition scheme for partial transmit sequence OFDM," *IEEE Trans. Broadcasting*, vol. 45, pp. 333 – 338, Sept. 1999.

[35] Kikkert, C., "Digital companding techniques," *IEEE Trans. Communications*, vol. 22, pp. 75–78, Jan. 1974.

[36] Kim, D. and Stuber, G. L., "Clipping noise mitigation for OFDM by decision-aided reconstruction," *IEEE Communications Letters*, vol. 3, pp. 4–6, 1999.

[37] Krongold, B. S. and Jones, D. L., "PAR reduction in OFDM via active constellation extension," *IEEE Trans. on Broadcasting*, vol. 49, pp. 258 – 268, Sept. 2003.

[38] Lei, X., Li, S., and Tang, Y., "OFDM clipping noise mitigation by a novel minimum clipping power loss scheme," *IEEE Proc. Vehicular Technology Conference*, vol. 4, pp. 2440 – 2443, Oct. 2003.

[39] Lim, D.-W., No, J.-S., Lim, C.-W., and Chung, H., "A new SLM OFDM scheme with low complexity for PAPR reduction," *IEEE Signal Processing Letters*, vol. 12, pp. 93 – 96, Feb. 2005.

[40] Mesdagh, D. and Spruyt, P., "A method to reduce the probability of clipping in DMT-based transceivers," *IEEE Trans. Communications*, vol. 44, pp. 1234–1238, Oct. 1996.

[41] Moose, P. H., "A technique for orthogonal frequency division multiplexing frequency offset correction," *IEEE Trans. Communications*, vol. 42, pp. 2908–2914, Oct. 1994.

[42] Muller, S. and Huber, J., "OFDM with reduced peak-to-average power ratio by optimum combination of partial transmit sequences," *IEE Electronics Letters*, vol. 33, pp. 368–369, Feb. 1997.

[43] Negi, R. and Cioffi, J., "Pilot tone selection for channel estimation in a mobile OFDM system," *IEEE Trans. on Consumer Electronics*, vol. 44, pp. 1122 – 1128, Aug. 1998.

[44] Ochiai, H. and Imai, H., "Multitone signals with low crest factor," *IEEE Trans. Circuits and System*, vol. 33, pp. 1018 – 1022, Oct. 1986.

[45] Ochiai, H. and Imai, H., "On the distribution of the peak-to-average power ratio in OFDM signals," *IEEE Trans. Communications*, vol. 49, pp. 282–289, Feb. 2001.

[46] Ochiai, H. and Imai, H., "Performance analysis of deliberately clipped OFDM signals," *IEEE Trans. Communications*, vol. 50, pp. 89 – 101, Jan. 2002.

[47] Ohkubo, N. and Ohtsuki, T., "Design criteria for phase sequences in selected mapping," *Proc. IEEE Vehicular Technology Conference*, vol. 1, pp. 373–377, Apr. 2003.

[48] O'Neill, R. and Lopes, L. B., "Envelope variations and spectral splatter in clipped multicarrier signals," *IEEE Proc. International Symposium on Personal, Indoor and Mobile Radio Communications*, vol. 1, pp. 71 – 75, Sept. 1995.

[49] Pollet, T., Bladel, M. V., and Moenaclaey, M., "BER sensitivity of OFDM systems to carrier frequency offset and wiener phase noise," *IEEE Trans. Communications*, vol. 43, pp. 191–192, Feb. 1995.

[50] Popovic, B. M., "Synthesis of power efficient multitone signals with flat amplitude spectrum," *IEEE Trans. Communications*, vol. 39, pp. 1031 – 1033, July 1991.

[51] Proakis, J. G., *Digital Communications*. New York, NY: McGraw-Hill, 2001.

[52] Qian, H. and Chen, N., "SLM distribution memo." Private communication, Oct. 2004.

[53] Qian, H., Xiao, C., Chen, N., and Zhou, G. T., "Dynamic selected mapping for OFDM," *Intl. Conference on Acoustics, Speech, and Signal Processing*, Mar. 2005.

[54] Rappaport, T., *Wireless Communications*. Prentice Hall, 2002.

[55] Russell, M. and Stuber, G. L., "Interchannel interference analysis of OFDM in a mobile environment," *Proc. IEEE Vehicular Technology Conference*, pp. 820–824, July 1995.

[56] Sathananthan, K. and Tellambura, C., "Partial transmit sequence arid selected mapping schemes to reduce ICI in OFDM systems," *IEEE Communications Letters*, vol. 6, pp. 313 – 315, Aug. 2002.

[57] Schroeder, M. R., *Number Theory in Science and Communication*. Berlin, Germany: Springer, 1997.

[58] Simon, M., *Probability Distributions Involving Gaussian Random Variables: A Handbook for Engineers and Scientists*. Norwell, MA: Kluwer Academic Publishers, 2002.

[59] Starr, T., Cioffi, J. M., and Silverman, P. J., *Understanding Digital Subscriber Line Technology*. Pearson Education, 1998.

[60] Tellado, J., *Multicarrier Modulation with Low PAR: Applications to DSL and Wireless*. Kluwer Academic Publishers, 2000.

[61] Tellado, J. and Cioffi, J. M., "Efficient algorithms for reducing PAR in multicarrier systems," *Proc. IEEE International Symposium on Information Theory*, p. 191, Aug. 1998.

[62] Valbonesi, L. and Ansari, R., "Peak-to-average power ratio reduction in OFDM: optimal and suboptimal combination of erasure pattern selection and probabilistic methods," *Canadian Conference on Electrical and Computer Engineering*, vol. 4, pp. 2175 – 2178, May 2004.

[63] van Nee, R. and de Wild, A., "Reducing the peak-to-average power ratio of OFDM," *Proc. IEEE Vehicular Technology Conference*, vol. 3, pp. 2072–2076, 1998.

[64] Wang, C.-L., , Ouyang, Y., and Hsu, M.-Y., "Low-complexity peak-to-average power ratio reduction techniques for OFDM systems." Submitted to *IEEE Transactions on Circuits and Systems - Part I*, 2004.

[65] Wang, X., Tjhung, T., and Ng, C., "Reduction of peak-to-average power ratio of OFDM system using a companding technique," *IEEE Trans. on Broadcasting*, vol. 45, pp. 303–307, Sept. 1999.

[66] Weinstein, S. B. and Ebert, P. M., "Data transmission by frequency division multiplexing using the discrete fourier transform," *IEEE Trans. Comm. Technology*, vol. COM-19, pp. 282–289, Oct. 1971.

[67] Weisstein, E. W., "Lambert w-function." http://mathworld.wolfram.com/LambertW-Function.html.

[68] Wulich, D., Dinur, N., and Glinowiecki, A., "Level clipped high-order OFDM," *IEEE Trans. on Communications*, vol. 48, pp. 928–930, June 2000.

[69] Zhou, G. T., Baxley, R. J., and Chen, N., "Selected mapping with monomial phase rotations for peak-to-average power ratio reduction in OFDM," *Proc. Intl. Conf. on Communications, Circuits and Systems*, June 2004.

[70] Zhou, G. T., Giannakis, G. B., and Swami, A., "On polynomial phase signals with time-varying amplitudes," *IEEE Trans. on Signal Processing*, vol. 44, no. 4, 1996.

[71] Zhou, G. T. and Peng, L., "Optimality condition for selected mapping in OFDM." Submitted to *IEEE Transactions on Signal Processing*, 2005.

[72] Zhou, G. T. and Wang, Y., "Exploring lag diversity in the high-order ambiguity function for polynomial phase signals," *IEEE Signal Processing Letters*, vol. 4, no. 8, 1997.

[73] Zou, W. Y. and Wu, Y., "COFDM: An overview," *IEEE Trans. Broadcasting*, vol. 41, pp. 1–8, March 1995.